

Global analysis of regulatory network dynamics: equilibria and saddle-node bifurcations

Shane Kepley*, Konstantin Mischaikow† and Elena Queirolo‡

May 2, 2022

Abstract

In this paper we describe a combined combinatorial/numerical approach to studying equilibria and bifurcations in network models arising in Systems Biology. Often interactions are only coarsely known in terms of a regulatory or signalling network topology. Consequently, ODE models of the dynamics suffer from high dimensional parameters which presents a significant obstruction to studying the global dynamics via numerical methods.

Given a network topology describing state variables which regulate one another via monotone and bounded functions, we first use the *Dynamic Signatures Generated by Regulatory Networks* (DSGRN) software to obtain a combinatorial description which summarizes the dynamics. This summary is coarse but global and we use this information as a first pass to identify “interesting” subsets of parameters in which to focus. We construct an associated ODE model with high parameter dimension using our *Network Dynamics Modeling and Analysis* (NDMA) Python library. We introduce algorithms for efficiently investigating the dynamics in these ODE models restricted to these parameter subsets. Finally, we perform a statistical validation of the method and several interesting dynamical applications including finding saddle-node bifurcations in a 54 parameter model.

1 Introduction

Consider an explicit system of differential equations

$$\dot{x} = f(x, \lambda), \quad x \in \mathbb{R}^N, \quad \lambda \in \mathbb{R}^M. \quad (1)$$

A natural goal is to understand the global dynamics over all parameter values. In general this goal is likely unreachable. A simpler problem is to choose a relevant invariant set, e.g. an equilibrium or periodic orbit, and identify the set of parameters at which this exists. This leads to the closely related problem of identifying specific types of bifurcations, i.e. set of parameters at which the above mentioned invariant sets change. In special cases, considerable progress has been made on these simpler problems, such as [19], and more general results presented in [9].

We refer to the question of existence and stability of equilibria as the *equilibrium problem*. If M , the dimension of parameter space, equals 1, then the equilibrium problem is often approached by identifying an equilibrium at a given parameter value and then using continuation

*s.kepley@vu.nl

†mischaik@math.rutgers.edu

‡elena.queirolo@tum.de

techniques to characterize the equilibrium as a function of λ and to identify bifurcation points, i.e. isolated points in parameter space where the equilibrium changes stability or disappears. This same strategy can be carried out when $M = 2$ though characterizing the equilibria is a challenge [4, 8] as one needs to identify a 2-dimensional surface of points in \mathbb{R}^N . Therefore, typically one settles for identifying the bifurcations. If these are saddle-node bifurcations (associated with the appearance and disappearance of equilibria), then generically they take the form of 1-dimensional curves that themselves can be identified via continuation.

The focus of this paper is in addressing the equilibrium problem, but for large M . Our analysis is carried out for a specific family of ODEs though in principle these techniques are much more broadly applicable. Observe that the immediate challenge is that bifurcations occur on higher dimensional surfaces. For example, generically saddle-node bifurcations will be associated with $M - 1$ -dimensional hypersurfaces and deriving an explicit representations for these hypersurface appears to be impossible. In fact, identifying even a single parameter on this hypersurface is already highly nontrivial. With this in mind, the goal of this paper is to describe techniques for finding such parameters.

The main idea is to consider the problem at two “resolutions”. First, we apply combinatorial methods which consider the dynamics coarsely. These methods have been implemented in the DSGRN library and have been previously used to systematically address modest, but still interesting questions about invariant sets and bifurcations in high dimensional parameter spaces. We discuss this in greater depth below. The second step is to use the information gained from this combinatorial analysis to guide a refined analysis of the dynamics using an ODE with high parameter dimension. Despite the high parameter dimension, we restrict to parameter subsets identified as “interesting” using DSGRN and perform these computations efficiently using our NDMA numerical library which incorporates several novel algorithms introduced in section 4.

Specifically, in this paper we demonstrate that for a broad family of differential equations we can efficiently propose paths in parameter space along which we expect to experience a saddle-node bifurcation and then check the veracity of this expectation. Stated differently, even though we do not know the $M - 1$ dimensional hypersurface along which the saddle-node bifurcations occur, we can suggest paths that we expect cross this hypersurface and then check if this is the case. Moreover, we believe that our approach is applicable to broader range of bifurcations and that it can be applied to a much wider class of nonlinearities.

A unique feature of our approach is the starting point: an explicit description in parameter space that *suggests* where the bifurcations of interest occur. To explain how this description is derived we begin with a brief discussion of software [2, 18, 6, 14], called Dynamic Signatures Generated by Regulatory Networks (DSGRN). Leaving the details to section 3 for the moment we note that the input to DSGRN is an annotated directed graph and a list of interaction functions (see section 2 for formal definitions). The output of DSGRN is an explicit finite decomposition of parameter space with the property that on each region of the decomposition there is a constant combinatorial representation of dynamics called a *Morse graph*. This decomposition is organized via the *parameter graph* where each node of the parameter graph represents a single region. An edge between two nodes indicates that the closure of the two associated regions intersect over a codimension one hypersurface. If the annotated directed graph has N nodes and E edges, then the associated parameter space is $\Xi = (0, \infty)^{N+3E}$.

For the sake of demonstration, in much of the discussion of this paper we will focus on a particularly simple annotated graph that represents the regulatory network commonly referred to as the *Toggle Switch*, shown in Figure 1(a). Taking the toggle switch as the input to DSGRN, the associated parameter space is $\Xi = (0, \infty)^8$. DSGRN decomposes Ξ into nine regions and the parameter graph for the toggle switch is shown in Figure 1(b).

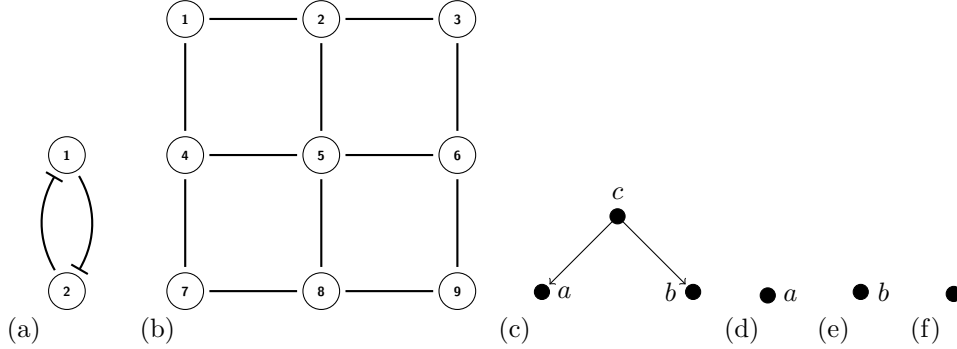


Figure 1: (a) Toggle switch. (b) Parameter graph for toggle switch. (c) Morse graph at node 5 of parameter graph. (d) Morse graph at nodes 1, 2, and 4 of parameter graph. Note that the element a of these Morse graph can be directly identified with the element a of the Morse graph at node 5. (e) Morse graph at nodes 6, 8, and 9 of parameter graph. Note that the element b of these Morse graph can be directly identified with the element b of the Morse graph at node 5. (f) Morse graph at nodes 3 and 7.

As indicated above a Morse graph is associated to each node in the parameter graph and the Morse graph provides a characterization of the global dynamics. More precisely a Morse graph is an acyclic directed graph or equivalently a partially ordered set (M, \leq) . The elements of the Morse graph represent potential recurrent dynamics and the partial order indicates the direction of the dynamics, i.e., if $p, q \in M$ and $p < q$, then no orbit can limit in backward time to the recurrent dynamics associated to p and in forward time to the recurrent dynamics associated to q .

Returning to the toggle switch, Figure 1(c)-(f) indicate the Morse graphs at different nodes of the parameter graph. An appropriate interpretation of this information is that at the parameter values associated with Node 5 (we denote this as $R(5)$), the system exhibits bistability where the elements a and b indicate the existence of distinct attractors and the element c indicates the existence of an unstable invariant set that acts as a separatrix between the two attractors. At the remaining parameter nodes, the Morse graph contains a single element suggesting that at the associated parameter values the dynamics is monostable.

Ignoring for the moment the meaning of the parameters, the third column of Table 1 provides the explicit decomposition of parameter space. There is an edge in the parameter graph between Node 5 and Node 2 and from Table 1 the reader can check that the shared boundary between the associated regions $R(5)$ and $R(2)$ is the 7 dimensional surface defined by

$$\ell_{1,2} = \gamma_1 \theta_{2,1}, \quad \ell_{2,1} < \gamma_2 \theta_{1,2} < \ell_{2,1} + \delta_{2,1}. \quad (2)$$

If the recurrent dynamics captured by the elements a , b , and c of the Morse graph at Node 5 are equilibria, then the change in dynamics between parameters in Node 5 and Node 2 is most easily associated with the occurrence of a saddle-node bifurcation, i.e., for each parameter value that lies on the hypersurface defined by (2) there exists a saddle-node bifurcation.

Node	Phenotype	Attractors	Inequalities	Reduced Inequalities
1	Monostable	$\{(1, 0)\}$	$\gamma_1\theta_{2,1} < \ell_{1,2} < \ell_{1,2} + \delta_{1,2}$ $\ell_{2,1} < \ell_{2,1} + \delta_{2,1} < \gamma_2\theta_{1,2}$	$1 < \ell_{1,2}$ $\ell_{2,1} + \delta_{2,1} < \gamma_2$
2	Monostable	$\{(1, 0)\}$	$\gamma_1\theta_{2,1} < \ell_{1,2} < \ell_{1,2} + \delta_{1,2}$ $\ell_{2,1} < \gamma_2\theta_{1,2} < \ell_{2,1} + \delta_{2,1}$	$1 < \ell_{1,2}$ $\ell_{2,1} < \gamma_2 < \ell_{2,1} + \delta_{2,1}$
3	Monostable	$\{(1, 1)\}$	$\gamma_1\theta_{2,1} < \ell_{1,2} < \ell_{1,2} + \delta_{1,2}$ $\gamma_2\theta_{1,2} < \ell_{2,1} < \ell_{2,1} + \delta_{2,1}$	$1 < \ell_{1,2}$ $\gamma_2 < \ell_{2,1}$
4	Monostable	$\{(1, 0)\}$	$\ell_{1,2} < \gamma_1\theta_{2,1} < \ell_{1,2} + \delta_{1,2}$ $\ell_{2,1} < \ell_{2,1} + \delta_{2,1} < \gamma_2\theta_{1,2}$	$\ell_{1,2} < 1 < \ell_{1,2} + \delta_{1,2}$ $\ell_{2,1} + \delta_{2,1} < \gamma_2$
5	Bistable	$\{(0, 1), (1, 0)\}$	$\ell_{1,2} < \gamma_1\theta_{2,1} < \ell_{1,2} + \delta_{1,2}$ $\ell_{2,1} < \gamma_2\theta_{1,2} < \ell_{2,1} + \delta_{2,1}$	$\ell_{1,2} < 1 < \ell_{1,2} + \delta_{1,2}$ $\ell_{2,1} < \gamma_2 < \ell_{2,1} + \delta_{2,1}$
6	Monostable	$\{(0, 1)\}$	$\ell_{1,2} < \gamma_1\theta_{2,1} < \ell_{1,2} + \delta_{1,2}$ $\gamma_2\theta_{1,2} < \ell_{2,1} < \ell_{2,1} + \delta_{2,1}$	$\ell_{1,2} < 1 < \ell_{1,2} + \delta_{1,2}$ $\gamma_2 < \ell_{2,1}$
7	Monostable	$\{(0, 0)\}$	$\ell_{1,2} < \ell_{1,2} + \delta_{1,2} < \gamma_1\theta_{2,1}$ $\ell_{2,1} < \ell_{2,1} + \delta_{2,1} < \gamma_2\theta_{1,2}$	$\ell_{1,2} + \delta_{1,2} < 1$ $\ell_{2,1} + \delta_{2,1} < \gamma_2$
8	Monostable	$\{(0, 1)\}$	$\ell_{1,2} < \ell_{1,2} + \delta_{1,2} < \gamma_1\theta_{2,1}$ $\ell_{2,1} < \gamma_2\theta_{1,2} < \ell_{2,1} + \delta_{2,1}$	$\ell_{1,2} + \delta_{1,2} < 1$ $\ell_{2,1} < \gamma_2 < \ell_{2,1} + \delta_{2,1}$
9	Monostable	$\{(0, 1)\}$	$\ell_{1,2} < \ell_{1,2} + \delta_{1,2} < \gamma_1\theta_{2,1}$ $\gamma_2\theta_{1,2} < \ell_{2,1} < \ell_{2,1} + \delta_{2,1}$	$\ell_{1,2} + \delta_{1,2} < 1$ $\gamma_2 < \ell_{2,1}$

Table 1: The result of the DSGRN analysis for the Toggle Switch. As indicated in Figure 1(b) DSGRN partitions the parameter space into 9 parameter regions which give rise to the nodes of the parameter graph. The Morse graph associated with each node gives rise to the phenotype. The inequalities column indicates the explicit region in parameter space associate to each node. For the reduced parameter space defined in Section 5.2, the corresponding parameter regions are the semi-algebraic subsets of Ξ^* described by the inequalities in the last column.

It is quite reasonable if by this point the reader is troubled by the fact that no particular dynamical system has been discussed, and yet, an explicit seven dimensional set of saddle-nodes is being proposed. This leads to two fundamental points.

1. DSGRN has been designed with the goal of characterizing dynamics for a broad class of dynamical systems as opposed to finding specific solutions to any particular system.
2. The hypersurface defined by (2) is meant to provide an educated guess as to where saddle-node bifurcations occur.

To quantify how useful (2) is requires that we consider a particular family of differential equations. For this paper we use Hill models (see section 2 for an explicit formulation). There are three reasons that we choose to work with these models.

1. They are expressed in terms of rational functions. As a consequence, a numerical library can be built that computes derivatives of the vector field up to any given order, with respect to both the phase space variables and any of the parameters. Therefore, this library provides a basis for rigorous validation of the numerically detected dynamics. The DSGRN parameter space embeds in a very natural way into the Hill model parameter space.
2. They arise naturally in the context of systems biology.

The Hill model for the toggle switch is given by

$$\begin{aligned}\dot{x}_1 &= -\gamma_1 x_1 + \ell_{1,2} + \delta_{1,2} \frac{\theta_{1,2}^{d_{1,2}}}{\theta_{1,2}^{d_{1,2}} + x_2^{d_{1,2}}} \\ \dot{x}_2 &= -\gamma_2 x_2 + \ell_{2,1} + \delta_{2,1} \frac{\theta_{2,1}^{d_{2,1}}}{\theta_{2,1}^{d_{2,1}} + x_1^{d_{2,1}}}\end{aligned}\tag{3}$$

which includes 10 parameters, $\{\gamma_1, \ell_{1,2}, \delta_{1,2}, \theta_{1,2}, d_{1,2}, \gamma_2, \ell_{2,1}, \delta_{2,1}, \theta_{2,1}, d_{2,1}\} \subset (0, \infty)$. The corresponding DSGRN parameters are $\{\gamma_1, \ell_{1,2}, \delta_{1,2}, \theta_{1,2}, \gamma_2, \ell_{2,1}, \delta_{2,1}, \theta_{2,1}\}$ and as first pass it is useful to think of DSGRN as capturing the dynamics of (3) in the singular limit as the exponents $d_{1,2}$ and $d_{2,1}$ go to infinity. In fact, there is a bijection between the equilibria identified by DSGRN and the equilibria for a Hill function model for sufficiently large exponents [3, Theorem 3.13]. In the case of the Toggle Switch these equilibria agree with the vertices of the Morse graphs.

While we believe that the ability of DSGRN to identify equilibria is of fundamental importance, it is worth noting that within the synthetic biology community the toggle switch represents a first successful design of a synthetic genetic switch [5]. For this community an abstract existence result invoking the phrase “sufficiently large exponents” is not of direct use as typical biochemical models involve Hill exponents d that are on the order of 5 or less. This brings us full circle and we ask the following questions. First, can we use the DSGRN information to provide intuition as to which parameter values will lead to bistability for (3)? Second, can we use this information to identify at what parameter values saddle-node bifurcations will occur. We note that the Morse graphs for a combinatorial network model typically encode a richer description of the global dynamical structure than simply the number and type of combinatorial attractors in each parameter region, such as the phase space region in which they occur. Analysis of the relative location of these attractors in “phase space” across multiple parameter regions may suggest subtle, yet global information about how these

attractors continue and which types of bifurcations occur. We demonstrate this in a specific example in section 6.2.

One of the aims of this paper is to develop a general procedure by which we can begin with the information from the DSGRN computations on the toggle switch and build up towards more complicated systems of ODEs. Figure 2 is meant to provide intuition concerning the approach we take. Consider an eight-dimensional slice of DSGRN parameter space Ξ through regions $R(4)$, $R(5)$, and $R(6)$. As indicated in Figure 1 DSGRN identifies bistability for $R(5)$ and monostability for $R(4)$ and $R(6)$. For simplicity we assume $d = d_{1,2} = d_{2,1}$. By [3] and as indicated by the gray regions the equilibria identified by DSGRN persist for d sufficiently large. Finally, for $d = 1$ equation (3) has a unique equilibrium. As a consequence the bistability exhibited in $R(5)$ for large d must fail for some value of $d > 1$. The generic expectation is that bistability is lost via a saddle-node bifurcation and thus there should be an nine-dimensional surface in Λ the parameter space for (3) on which this bifurcation occurs. Two simplified scenarios for the structure of this surface are shown in Figure 2: the solid curve and the dashed curve. The solid curve is meant to suggest that if a saddle-node bifurcation occurs then the Ξ parameters lie in $R(5)$, whereas the dashed curve suggest that the Ξ parameters may lie in $R(4)$ or $R(6)$.

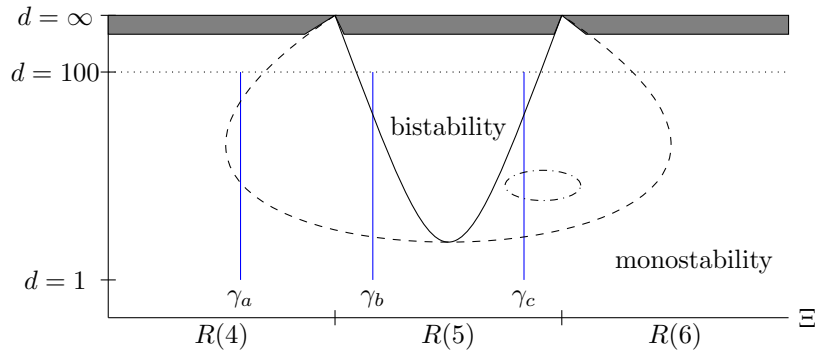


Figure 2: Schematic description of the strategy of this paper. $R(4)$, $R(5)$, and $R(6)$ are regions of parameter space Ξ identified by DSGRN for Toggle switch. As indicated in Figure 1 DSGRN identifies bistability for $R(5)$ and monostability for $R(4)$ and $R(6)$. We are interested in understanding the equilibrium structure for (3). Set $d = d_{1,2} = d_{2,1}$. By [3] and as indicated by the gray regions the equilibria identified by DSGRN persist for d sufficiently large. For $d = 1$ (3) has a unique equilibrium. There therefore must be an interface between the monostability region and the bistability region. In this paper, we justify that the main mechanism to pass from monostability to bistability is through a saddle node bifurcation and we investigate the “shape” of the boundary between stability regions.

The remainder of this paper is organized as follows. In section 2, the notation and structure of Hill models is introduced. While the core ideas of this paper are model-independent, and only rely on smooth approximations of step functions, the implementation is not and a choice for the class of ODE models is required. Our implementation in the NDMA library is based on Hill functions due to their compatibility with the combinatorial dynamical models used in DSGRN. In section 3 we review the basics of the DSGRN software for readers who may not be familiar with it.

In section 4 we consider the numerical equilibrium and saddle-node bifurcation problems

for Hill models. Both are characterized as zero finding problems. Additionally, we introduce an algorithm for obtaining a-prior bounds on equilibria and isolating them based on the so called “radii polynomials”. In section 5.1 we carefully describe the entire combinatorial/numerical approach for the Toggle Switch example and perform a statistical validation of its effectiveness in characterizing equilibria and saddle-node bifurcations in this model.

We conclude the paper with three examples which demonstrate effectiveness of our strategy to bifurcation analysis. These examples include further analysis of the Toggle Switch example as well as a 54 parameter model of the Epithelial-Mesenchymal Transition (EMT) network which is of practical importance. In this example, the high parameter dimension makes it essentially impossible to predict the number of stable equilibria or observe a saddle-node bifurcation by randomly choosing parameters. Nevertheless, we demonstrate that we can efficiently do both.

2 Hill models

In this section we provide a formal definition of the Hill models considered in this paper. We begin by noting that Hill models take the form

$$\dot{x} = -\Gamma x + \mathcal{H}(x), \quad x \in [0, \infty)^N \quad (4)$$

where Γ is a diagonal matrix with $\Gamma_{ii} = \gamma_i > 0$. The rest of this section is dedicated to defining the nonlinear function \mathcal{H} . This requires several preliminary constructions that are imposed so that there is an obvious correspondence between the computations that DSGRN is currently capable of performing and the form of the Hill models.

Definition 1. An *activating Hill response* is a function $H^+ : [0, \infty) \rightarrow [0, \infty)$ given by

$$H^+(x) := \ell + \delta \frac{x^d}{\theta^d + x^d}$$

and a *repressing Hill response* is a function $H^- : [0, \infty) \rightarrow [0, \infty)$ given by

$$H^-(x) := \ell + \delta \frac{\theta^d}{\theta^d + x^d}$$

where the parameters $\{\ell, \delta, \theta, d\}$ are positive and $d \geq 1$.

We refer to the parameter d as the *Hill exponent*.

In biological applications, Hill models are extensively used for modeling the internal behaviour of the cell [5, 17, 21]. They are coupled with the study of network dynamics, as presented in [18], where a repressing edge is associated with H^- and an activating edge with H^+ .

Observe that H^+ is monotonically increasing and satisfies

$$H^+(0) = \ell \quad \lim_{x \rightarrow \infty} H^+(x) = \ell + \delta.$$

Similarly, H^- is monotonically decreasing and satisfies

$$H^-(0) = \ell + \delta \quad \lim_{x \rightarrow \infty} H^-(x) = \ell.$$

In general \mathcal{H} is a function of multiple variables and in what follows we indicate how \mathcal{H} can be constructed from activating and repressing Hill responses.

Definition 2. A polynomial, $p \in \mathbb{R}[z_1, \dots, z_N]$ is called an *interaction function* if it has the form

$$p = \prod_{m=1}^q p_m, \quad \text{where} \quad p_m = \sum_{j \in I_m} z_j,$$

and $\{I_1, \dots, I_q\}$ is a partition of the integers, $\{1, \dots, N\}$.

Interaction functions allow us to define Hill models.

Definition 3. A *Hill model* is a system of differential equations $\dot{x} = f(x)$, $x \in [0, \infty)^N$ such that for each $i \in \{1, \dots, N\}$,

$$\dot{x}_i = f_i(x) = -\gamma_i x_i + \mathcal{H}_i(x) \quad (5)$$

where

$$\mathcal{H}_i(x) = p_i(H_{i,1}^*(x_1), \dots, H_{i,N}^*(x_N)) \quad (6)$$

for some interaction function p_i .

Though suppressed in the notation presented above Hill models involve a multitude of parameters. In particular, each variable x_i contributes a parameter γ_i and x_j influencing the rate of change of x_i contributes four parameters $\ell_{i,j}$, $\delta_{i,j}$, $\theta_{i,j}$, and $d_{i,j}$. Occasionally, ordering these parameters is relevant. In this case we express the parameter vector as $\lambda = (\gamma, \ell, \delta, \theta, d)$ where the ordering on the vectors γ , ℓ , δ , θ , and d is lexicographic with respect the ordering of the nodes. For fixed parameter λ we will write the Hill model as

$$\dot{x} = f(x, \lambda).$$

3 DSGRN

As indicated in the introduction DSGRN [18] is a software designed to analyze the global dynamics of gene regulatory networks. There is substantial mathematical theory underpinning the development of DSGRN [10, 13, 11, 12], however for the purposes of this paper we treat it as a black box.

The input to the software is an annotated directed graph (\mathcal{G}, p) , e.g. Figure 1(a), with N nodes, E edges indicating activation or repression, and a vector of choices of interaction functions $p = (p_1, \dots, p_N)$, where p_n is the interaction function applied at node n . To each such graph DSGRN ascribes a parameter space $\Xi := (0, \infty)^{N+3E}$ with parameters $\{\gamma, \ell, \delta, \theta\}$. The Hill models described in Section 2 are based on these parameters plus the Hill exponents $d \in (0, \infty)^E$.

Remark 1. To match a Hill model with DSGRN, one interprets the edges of the annotated graph (\mathcal{G}, p) as

$$H_{i,j}^* = \begin{cases} H_{i,j}^+ & \text{if } j \rightarrow i \\ H_{i,j}^- & \text{if } j \dashrightarrow i \\ 0 & \text{otherwise.} \end{cases}$$

The output is the DSGRN database that is best understood conceptually as an annotated graph that we refer to as a *parameter graph* and denote by $PG(\mathcal{G}, p)$. Each node v of $PG(\mathcal{G}, p)$ corresponds to a semi-algebraic set $R(v) \subset \Xi = (0, \infty)^{N+3E}$ given in terms of explicit inequalities, and the union of closures of all these semi-algebraic sets is $\Xi = [0, \infty)^{N+3E}$. If two nodes v and v' share an edge in the parameter graph, then their expressions as semi-algebraic

sets differs by exactly one inequality, and in particular $\text{cl}(R(v)) \cap \text{cl}(R(v'))$ is a codimension 1 hypersurface in $\Xi = (0, \infty)^{N+3E}$.

In addition, the DSGRN database assigns to each node v a partially ordered set $(\mathbf{M}(v), \leq_v)$, that is visually expressed via the Hasse diagram and called the *Morse graph* at parameter node v . Given a particular choice of parameter values $\lambda = (\gamma, \ell, \delta, \theta, d)$ if $(\gamma, \ell, \delta, \theta) \in R(s)$, then under the assumption that each coordinate of d is sufficiently large we claim the Morse graph provides a useful combinatorial representation of the global dynamics of the associated Hill model $\dot{x} = f(x, \lambda)$.

To provide at least some intuition (see [2, 7, 3] for details) into content of this assertion we provide a minimal amount of information about the internal workings of DSGRN. Returning to Definition 1 observe that H^+ and H^- converge to step functions

$$\begin{cases} \ell & \text{if } \xi < \theta \\ \ell + \delta & \text{if } \xi > \theta \end{cases} \quad \text{and} \quad \begin{cases} \ell + \delta & \text{if } \xi < \theta \\ \ell & \text{if } \xi > \theta, \end{cases}$$

respectively, as $d \rightarrow \infty$. Thus, in this singular limit the thresholds θ indicate the locations in phase space where the dynamics changes. DSGRN exploits this by decomposing phase space $\Xi = (0, \infty)^N$ into a cubical complex defined by the hyperplanes $x_i = \theta_{j,i}$ for any edge i to j in the regulatory network. DSGRN models the dynamics via a directed graph, called the *state transition graph* that identifies how cells are mapped to adjacent cells (a self loop indicates that the cell is mapped to itself). There is a single state transition graph associated to each node s in the parameter graph. DSGRN compresses the information in the state transition graph by identifying the recurrent strongly connected path components, i.e. the strongly connected path components that contain at least one edge. There is a 1-1 correspondence between the recurrent strongly connected path components and the elements of $\mathbf{M}(s)$. Furthermore, given $p, q \in \mathbf{M}(s)$, $p \leq_s q$ implies that there exists a path in the state transition graph from the strongly connect path component associated with q to the strongly connect path component associated with p .

Observe that if a cell in the state transition graph has a self edge, then that cell must belong to a recurrent strongly connected path component. Furthermore, at least conceptually, the existence of a self edge suggests the existence of a fixed point. With this in mind if $p \in \mathbf{M}(s)$ arises from a recurrent strongly connected path component that contains exactly one cell from the cubical complex, then DSGRN labels p as an *FP*. In particular, if p is a minimal element of $\mathbf{M}(s)$ and labeled as an *FP*, then the expectation is that p identifies a stable fixed point.

As is indicated in the introduction we are interested in identifying bifurcations to differential equations. Since a formal definition of bifurcation involves a change in the structure of an invariant set, DSGRN is incapable of directly identifying bifurcations. Nevertheless changes in the Morse graphs as a function of parameter nodes strongly suggest that the dynamics for associated differential equations should also changes. Thus, for the purpose of this paper, we introduce the following definition.

Definition 4. Let (\mathcal{G}, p) be an annotated graph with a vector of interaction functions and let $PG(\mathcal{G}, p)$ be the associated parameter graph. A DSGRN *saddle-node bifurcation edge* is an edge (v_1, v_2) in $PG(\mathcal{G}, p)$ such that the number of minimal FP in $\mathbf{M}(v_1)$ and $\mathbf{M}(v_2)$ differs by exactly one and the number of nonminimal FP in $\mathbf{M}(v_1)$ and $\mathbf{M}(v_2)$ differs by exactly one.

4 Equilibria and Saddle-node Bifurcations

Our strategy for identifying saddle-node bifurcations for (1) involves four steps.

Step 1 Choose a parameterized path $\mathbf{r}: [0, 1] \rightarrow \Lambda$ along which we expect a saddle-node bifurcation to occur.

Step 2 Subdivide $[0, 1]$ at points $0 = s_0 < \dots < s_i < \dots < s_I = 1$ and identify equilibria of (1) at parameter value $\mathbf{r}(s_i)$.

Step 3 If the number of equilibria for f at $\mathbf{r}(s_i)$ and $\mathbf{r}(s_{i+1})$ differs, then a refined search takes place to precisely determine where a bifurcation should take place.

Step 4 If any candidates are identified in step 3, we apply the algorithm outlined in this section to numerically find the saddle-node bifurcation with higher precision.

Remark 2. **Step 3** requires, in usual circumstances, to apply a continuation algorithm to the equilibria. Such algorithm then would detect the presence of saddles. In the case of Hill models, continuation algorithms are not ideal when the Hill coefficient is a free parameter. Indeed, continuing equilibrium branches with respect to the Hill coefficient is a stiff problem: far from a saddle node bifurcation, the equilibria move little in phase space, while close to saddle nodes significant changes occur depending on small changes of the Hill coefficient. This results in unreliable numerical continuation. For this reason, a bisection algorithm has also been implemented, that results in a cruder approach, but has proven to be not only more reliable but also faster than its continuation counterpart.

Observe that to effectively carry out this strategy requires that we be able to perform four tasks. First, we need to be able to make an informed guess concerning the path \mathbf{r} . As indicated in the introduction we choose curves along which the DSGRN parameter $\xi \in \Xi$ is constant, i.e. only the Hill coefficients are allowed to vary. To further simplify things, for all examples in this work we have chosen to identify all Hill coefficients and consider curves for which this single shared Hill coefficient ranges between 1 and 100. This choice has been made in the interest of simplicity, and it is not a constraint of the method nor of the library we are discussing.

As a result of the experiments of this paper we propose that if the ODE of interest is a Hill model (4), then ξ should be chosen to belong to a region for which the associated DSGRN Morse graph indicates multistability. Such region should be adjacent to at least one region that possesses a different number of equilibria. We expect this choice to be driven by the application at hand, thus it is beyond the scope of this paper to discuss it in further depth.

Second, we need an algebraic problem that defines a saddle-node bifurcation. For a definition of a saddle node bifurcation and analytic conditions that guarantee its existence we refer the reader to [1, Section 8.2] and [1, Theorem 8.12], respectively. Theorem 1 [15] presented below provides a means by which we can numerically find that a saddle node bifurcation occurs.

Theorem 1. *Consider a smooth one parameter family of ODEs,*

$$\dot{x} = g(x, s), \quad x \in \mathbb{R}^N, s \in \mathbb{R}.$$

Define $G : \mathbb{R}^{2N+1} \rightarrow \mathbb{R}^{2N+1}$ by

$$G(x, v, s) := \begin{pmatrix} g(x, s) \\ D_x g(x, s)v \\ v^T v - 1 \end{pmatrix} \quad x, v \in \mathbb{R}^N, s \in \mathbb{R}. \quad (7)$$

Let $u = (x, v, s) \in \mathbb{R}^{2N+1}$ and suppose $\hat{u} := (\hat{x}, \hat{v}, \hat{s})$ is a root of G satisfying

- 1. $D_u G(\hat{u})$ is an isomorphism.*

2. Every nonzero eigenvalue of $D_x g(\hat{x}, \hat{s})$ has nonzero real part.

Then g undergoes a saddle-node bifurcation at (\hat{x}, \hat{s}) and $\ker D_x g(\hat{x}, \hat{s}) = \text{span}\{\hat{v}\}$.

Remark 3. It is possible to use this Theorem, in combination with validation techniques, to *prove* the existence of a saddle node bifurcation. This lies beyond the scope of this paper, but the interested reader can refer to [15] for additional details. All computational elements needed for the validation of a Hill model are included in NDMA.

Third, identification of equilibria is a well studied but nontrivial problem. We exploit the structure of Hill models and provide an algorithm (see Algorithm 2) that identifies regions in phase space in which the equilibria must occur. This is discussed in Section 4.2.

Fourth, we identify numerical equilibria. From the previous, we can (and do) obtain different numerical representations for the same equilibrium. Furthermore, near the saddle-node bifurcation distinct equilibria can be nearly the same and we need to be able to insure that they are distinct. We resolve these issues with Algorithm 3 discussed in Section 4.3. Thus, the main focus of this Section is the development of **Step 2**, in particular the identification of all equilibria. While we are not claiming that our algorithm is fail proof, we claim it to be reliable. This Section will present the details of such search, first presenting an overview of the algorithm, and then going into more detail on the two key steps, comprised of a root finding algorithm for Hill models in Section 4.2 and a method to identify numerical equilibria in Section 4.3.

Throughout this section we suppose $\lambda \in \Lambda$ is fixed, $f : X \rightarrow TX$ is a Hill model with $X \subset \mathbb{R}^N$, and $\hat{x} \in \mathbb{R}^N$ is an equilibrium solution i.e. $f(\hat{x}) = 0$.

4.1 Overview of equilibrium finding

Within Step 2, we are asked to numerically find all equilibria for a given parameter value. In this Section, we give an initial overview of our method. We first assume implementations of two black box algorithms. The first is a root finding implementation which we denote by **FindRoot**, which takes a function, $f : \mathbb{R}^N \rightarrow \mathbb{R}^N$, and an initial guess $x_0 \in \mathbb{R}^N$ as input and attempts to identify a root of f near x_0 . When successful it returns $\hat{x} \in \mathbb{R}^N$ satisfying $\|f(\hat{x})\| \approx 0$. For the computations in this work we used a Newton based root finder but other options exist of course.

The second algorithm, denoted by **Unique**, identifies pairs of distinct vectors in \mathbb{R}^N which approximate the same root of f . That is, if \hat{x}_1, \hat{x}_2 satisfy

$$\|f(\hat{x}_1)\| \approx 0 \approx \|f(\hat{x}_2)\| \quad \text{and} \quad \|\hat{x}_1 - \hat{x}_2\| \approx 0,$$

then **Unique**(f, \hat{x}_1, \hat{x}_2) = \hat{x}_1 . If **Unique** does not identify \hat{x}_1 and \hat{x}_2 as zeros of f , then we say that they are *approximately* distinct with respect to f .

If \hat{x} is an array of vectors in \mathbb{R}^N and f a function from \mathbb{R}^N to itself, then **Unique**(f, \hat{x}) returns an new array of vectors in \mathbb{R}^N of size equal or smaller than \hat{x} , in which each pair of vectors is approximately distinct.

It is worth noting that Hill functions are trivially bounded, thus for any Hill model, there exists a rectangular subset of X of the form

$$R := \prod_{i=1}^N [a_i, b_i], \quad [a_i, b_i] \subset (0, \infty) \text{ for all } 1 \leq i \leq N. \quad (8)$$

such that all the zeros of the Hill model are within this rectangle. Furthermore, computing the bounds of R is trivial. The details are presented in Section 4.2.

With both **FindRoot**, R and **Unique** in hand, we can present the algorithm for the computation of all (up to numerical error) zeros of the Hill model f . Each interval in the product (8) is partitioned into k subintervals bounded by $k + 1$ uniformly spaced nodes. The product of these nodes forms a grid of points in \mathbb{R}^N which covers R . Each of the $(k + 1)^N$ points in this grid is taken as an initial condition for **Findroot** which attempts to return a candidate equilibrium nearby. The algorithm returns an array containing such candidates which are not identified as equivalent by **Unique**. The pseudocode is described in Algorithm 1.

Algorithm 1 General algorithm

```

1: function HillEquilibria( $f, R, k$ )
2:    $\hat{x} \leftarrow ()$  ▷ Initialize equilibrium array
3:    $\Delta_i \leftarrow \frac{b_i - a_i}{k}$ 
4:    $u_i \leftarrow (a_i, a_i + \Delta_i, \dots, a_i + (k - 1)\Delta_i, b_i)$  ▷ Discretize factors
5:   for  $\kappa \in \{1, \dots, k\}^N$  do
6:      $x_0 \leftarrow (u_{1,\kappa_1}, \dots, u_{N,\kappa_N})$ 
7:      $r_\kappa \leftarrow \text{FindRoot}(f, x_0)$  ▷ Returns a candidate when it converges
8:     if  $r_\kappa$  then  $\hat{x}.\text{Append}(r_\kappa)$  ▷ Append candidate equilibrium
9:   end if
10: end for
11: return  $\text{Unique}(f, \hat{x})$ 
12: end function

```

4.2 The bootstrap algorithm

In this section we define a second algorithm which exploits the structure of Hill models in specific cases to localize equilibria more reliably and efficiently than the Newton-based algorithm described above. The main idea is to begin with an initial rectangular subset of $(0, \infty)^N$ which is an enclosure for all equilibria and then iteratively obtain tighter rectangular enclosures by “bootstrap”.

Definition 5. We say that a continuous function $g: [0, \infty)^N \rightarrow (0, \infty)^N$ has a *monotone factorization* if for each $i = 1, \dots, N$, g_i factors as

$$g_i(x) = g_i^+(x)g_i^-(x) \quad \text{for all } x \in [0, \infty)^N,$$

where $g_i^+: [0, \infty)^N \rightarrow (0, \infty)^N$ is bounded and strictly increasing with respect to x_1, \dots, x_N and similarly, $g_i^-: [0, \infty)^N \rightarrow (0, \infty)^N$ is bounded and strictly decreasing with respect to x_1, \dots, x_N .

Consider a continuous function $f: [0, \infty)^N \rightarrow \mathbb{R}^N$ of the form $f(x) = -\Gamma x + g(x)$ where $g: [0, \infty)^N \rightarrow (0, \infty)^N$ has a monotone factorization and for all $i = 1, \dots, N$, $f_i(x) = -\gamma_i x + g_i(x)$ and $\gamma_i > 0$. Define $\Phi: \mathbb{R}^{2N} \rightarrow \mathbb{R}^{2N}$ coordinate-wise by the formulas

$$\Phi_i(\alpha, \beta) = \frac{1}{\gamma_i} g_i^+(\alpha) g_i^-(\beta) \quad \text{and} \quad \Phi_{N+i}(\alpha, \beta) = \frac{1}{\gamma_i} g_i^+(\beta) g_i^-(\alpha), \quad i = 1, \dots, N$$

where $\alpha, \beta \in \mathbb{R}^N$.

Theorem 2. Consider f , and Φ as defined above. Assume that $\liminf_{\|x\| \rightarrow \infty} g_i^-(x) > 0$ for all $i = 1, \dots, N$. Then, the following are true.

(i) $x \in [0, \infty)^N$ is a zero of f if and only if $(x, x) \in [0, \infty)^{2N}$ is a fixed point of Φ .

(ii) Define $(\alpha^{(0)}, \beta^{(0)}) \in \mathbb{R}^{2N}$ coordinate-wise by

$$\alpha_i^{(0)} := \frac{1}{\gamma_i} g_i^+(0) \liminf_{\|x\| \rightarrow \infty} g_i^-(x) \quad \text{and} \quad \beta_i^{(0)} := \frac{1}{\gamma_i} \limsup_{\|x\| \rightarrow \infty} g_i^+(x) g_i^-(0) \quad (9)$$

and iteratively define $(\alpha^{n+1}, \beta^{n+1}) = \Phi(\alpha^n, \beta^n)$ for $n \geq 1$. Then, $(\hat{\alpha}, \hat{\beta}) := \lim_{n \rightarrow \infty} (\alpha^n, \beta^n)$ exists.

(iii) If $f(\hat{x}) = 0$, then

$$\hat{\alpha}_i \leq \hat{x}_i \leq \hat{\beta}_i, \quad \text{for all } i = 1, \dots, N.$$

Proof. We leave it to the reader to check (i). (ii) follows from the boundedness and strict monotonicity of g_i^+ and g_i^- . To be more specific, we prove inductively that for $1 \leq i \leq N$, $\alpha_i^{(n)}$ and $\beta_i^{(n)}$ are monotonically increasing and decreasing sequences, respectively. The base case follows from easy estimates

$$\alpha_i^{(1)} = \Phi_i(\alpha^{(0)}, \beta^{(0)}) = \frac{1}{\gamma_i} g_i^+(\alpha^{(0)}) g_i^-(\beta^{(0)}) > \frac{1}{\gamma_i} g_i^+(0) \liminf_{\|x\| \rightarrow \infty} g_i^-(x) = \alpha_i^{(0)}$$

and

$$\beta_i^{(1)} = \Phi_{N+i}(\alpha^{(0)}, \beta^{(0)}) = \frac{1}{\gamma_i} g_i^+(\beta^{(0)}) g_i^-(\alpha^{(0)}) < \frac{1}{\gamma_i} \limsup_{\|x\| \rightarrow \infty} g_i^+(x) g_i^-(0) = \beta_i^{(0)}.$$

Now assume that $\alpha_i^{(n)} < \alpha_i^{(n-1)}$ and $\beta_i^{(n)} > \beta_i^{(n-1)}$. The strict monotonicity of g_i^+ and g_i^- implies that

$$\alpha_i^{(n+1)} = \Phi_i(\alpha^{(n)}, \beta^{(n)}) = \frac{1}{\gamma_i} g_i^+(\alpha^{(n)}) g_i^-(\beta^{(n)}) > \frac{1}{\gamma_i} g_i^+(\alpha^{(n-1)}) g_i^-(\beta^{(n-1)}) = \alpha_i^{(n)}$$

and

$$\beta_i^{(n+1)} = \Phi_{N+i}(\alpha^{(n)}, \beta^{(n)}) = \frac{1}{\gamma_i} g_i^+(\beta^{(n)}) g_i^-(\alpha^{(n)}) < \frac{1}{\gamma_i} g_i^+(\beta^{(n-1)}) g_i^-(\alpha^{(n-1)}) = \beta_i^{(n)}.$$

The proof of (iii) is also done inductively. Define

$$\mathcal{R}^{(n)} := \prod_{i=1}^N [\alpha_i^{(n)}, \beta_i^{(n)}].$$

By the proof of (ii), $\mathcal{R}^{(n+1)} \subset \mathcal{R}^{(n)}$. Define $F : [0, \infty)^N \rightarrow [0, \infty)^N$ by the formula

$$F_i(x) = \frac{1}{\gamma_i} g_i(x) \quad 1 \leq i \leq N.$$

Observe that if $f(\hat{x}) = 0$, then $F(\hat{x}) = \hat{x}$. Therefore, it suffices to prove that if $F(\hat{x}) = \hat{x}$ then $\hat{x} \in \mathcal{R}^{(n)}$ for all $n \in \mathbb{N}$.

Observe that from the definitions of F and $(\alpha^{(0)}, \beta^{(0)})$,

$$F([0, \infty)^N) = \mathcal{R}^{(0)}$$

and therefore $\hat{x} \in \mathcal{R}^{(0)}$.

Inductively, suppose that $n \in \mathbb{N}$ is fixed and $\hat{x} \in \mathcal{R}^{(n-1)}$, i.e.

$$\alpha_i^{(n-1)} \leq \hat{x}_i \leq \beta_i^{(n-1)} \quad \text{for } 1 \leq i \leq N. \quad (10)$$

The inequalities of (10) combined with the definition of Φ implies that for all $1 \leq i \leq N$

$$\alpha_i^{(n)} = \frac{1}{\gamma_i} g_i^+ \left(\alpha^{(n-1)} \right) g_i^- \left(\beta^{(n-1)} \right) \leq F_i(\hat{x}) = \hat{x}_i \leq \frac{1}{\gamma_i} g_i^+ \left(\beta^{(n-1)} \right) g_i^- \left(\alpha^{(n-1)} \right) = \beta_i^{(n)}$$

where the inequalities are obtain from the fact that g_i^+ and g_i^- are strictly monotonically increasing and decreasing respectively. Therefore, $\hat{x} \in \mathcal{R}^{(n)}$. \square

Observe that $F(\mathcal{R}^{(n-1)}) = \mathcal{R}^{(n)}$.

This motivates the following algorithm for bounding equilibria.

Algorithm 2 Bootstrap algorithm

```

1: function RootEnclosure( $f$ )
2:    $u \leftarrow (\alpha^{(0)}, \beta^{(0)})$  ▷ Initialize orbit as described in Theorem 2
3:    $v \leftarrow \Phi(u)$ 
4:   while  $\|u - v\| > \epsilon$  do
5:      $u \leftarrow v$ 
6:      $v \leftarrow \Phi(u)$ 
7:   end while
8:    $R \leftarrow \prod_{i=1}^N [v_i, v_{N+i}]$ 
9:   return  $R$ 
10: end function
11: function MonotoneHillEquilibria( $f, k$ )
12:    $R \leftarrow \text{RootEnclosure}(f)$ 
13:   return HillEquilibria( $f, R, k$ )
14: end function

```

4.3 Isolating equilibria

Let us consider the situation in which the previous Sections equilibrium finding numerical algorithms return two solutions \bar{x}_1 and \bar{x}_2 . It is possible that they are two numerical representations of the same analytic solution, or that they represent two different analytic solutions. The numerical radii polynomial approach can allow us a heuristic to make this distinction.

The radii polynomial approach, as presented in [9, 16], is usually implemented rigorously for the validation of zero finding problems. In this Section, we are only interested in an approximate implementation, thus our results do not have status of proofs, contrary to the references given.

While it is possible to attempt a validation of any of the equilibria or saddle-node bifurcations found in this work, this is not the focus of the present work and we have not implemented it here. Validation of a single equilibrium or saddle-node bifurcation using the radii polynomial approach requires a given high precision numerical solution. It does not provide a means for producing such a solution which is the focus in this paper.

The radii polynomial approach is build around the contraction mapping theorem. In an abstract setting, we consider a zero-finding problem $F(x) = 0$. In our setting, $F = h(\cdot, \lambda)$ is the vector field associated with a Hill model, but the discussion in this section is presented in

a more general way. Suppose \bar{x} is an approximate root of F and A is an approximate inverse of the Jacobian of F at \bar{x} i.e. informally we assume

$$\|F(\bar{x})\| \approx 0 \quad \|A - DF(\bar{x})^{-1}\| \approx 0.$$

Then we define a “Newton-like” operator by the formula

$$T(x) = x - AF(x), \tag{11}$$

with the idea that if \bar{x} and A are sufficiently good approximations, then T is expected to be a contraction in some neighborhood of \bar{x} . To estimate the radius of contraction of T , we make use of the following theorem.

Theorem 3. *Let \bar{x}, A be given and T as defined in Equation (11). Suppose $Y > 0$ and $Z : (0, \infty) \rightarrow (0, \infty)$ satisfy the bounds*

$$Y \geq \|T(\bar{x}) - \bar{x}\|, \quad Z(r) \geq \max_{b \in B_1(0)} \|DT(\bar{x} + rb)\|,$$

then, let us define the radii polynomial as

$$p(r) = Y + (Z(r) - 1)r. \tag{12}$$

If there exists an r^* such that $p(r^*) < 0$, then there exists a unique \hat{x} such that $F(\hat{x}) = 0$ and $\|\bar{x} - \hat{x}\| < r^*$.

For the proof we refer to [9].

It is useful to first simplify

$$\|T(\bar{x}) - \bar{x}\| = \|AF(\bar{x})\| = Y,$$

thus Y can be computed straightforwardly.

In our case, we notice $DT(x) = I - ADF(x)$, thus

$$DT(\bar{x} + rb) = I - ADF(\bar{x} + rb) = I - ADF(\bar{x}) + A(DF(\bar{x}) - DF(\bar{x} + rb))$$

and we split to computation of $Z(r)$ into the computation of $Z_0 \geq \|I - ADF(\bar{x})\|$ and $Z_1(r) \geq \max_{b \in B_1(0)} \|A(DF(\bar{x}) - DF(\bar{x} + rb))\|$. It's worth noting that

$$\max_{b \in B_1(0)} \|A(DF(\bar{x}) - DF(\bar{x} + rb))\| \leq \max_{z, b \in B_1(0)} \|AD^2F(\bar{x} + rz)b\|r.$$

We then approximate $\max_{z, b \in B_1(0)} \|AD^2F(\bar{x} + rz)b\|r \approx \|AD^2F(\bar{x})\|r := Z_1r$, by assuming that the second derivative of F is almost constant. While the approximation is crude, it has proven to be sufficiently precise for the task of identifying equivalent equilibria.

We then have the radii polynomial as

$$p(r) = Y + (Z_0 + Z_1r - 1)r,$$

and the biggest existence radius is

$$r^* = \frac{1 - Z_0 + \sqrt{Z_1^2 - 4(Z_0 - 1)Y}}{2Z_1}.$$

With this approach in mind, we can distinguish between numerical duplicates of equilibria and multiple equilibria. Considering the numerical approximations \bar{x}_1, \bar{x}_2 of equilibria, we

can compute their associated (approximate) existence radii r_1^*, r_2^* . If $\|\bar{x}_1 - \bar{x}_2\| < \max(r_1^*, r_2^*)$, then we consider them to be numerical duplicates, otherwise, they represent different analytical solutions. We can then expand this algorithm to a set of approximate equilibria $\{\bar{x}_1, \dots, \bar{x}_n\}$. First, all radii $r_i^*, i = 1, \dots, n$ are computed, then we delete any x_i such that there is an x_j with $\|x_i - x_j\| < \max(r_i^*, r_j^*)$. To reduce the number of comparisons, we restrict ourselves to $j < i$.

We implement `RadiiPol` as a function that computes r^* for any function f and approximate equilibrium \bar{x} .

Algorithm 3 Unique algorithm

```

1: function Unique( $f, X$ )
2:   for  $\bar{x} \in X$  do
3:      $r \leftarrow \text{RadiiPol}(f, \bar{x})$ 
4:     if  $\bar{y} \in X: \|\bar{x} - \bar{y}\| < r$  then
5:       delete  $\bar{y}$  from  $X$ 
6:     end if
7:   end for
8:   return  $X$ 
9: end function

```

5 The Toggle Switch

In this section we present the analysis for the Toggle Switch example discussed in in Section 1 and shown in Figure 1(a). We have chosen this example because the Toggle Switch is the one of the simplest network motifs which exhibits both monostability and bistability. Indeed, both the combinatorial Toggle Switch analyzed using DSGRN and the Toggle Switch Hill model analyzed using NDMA generically exhibit two dynamic phenotypes depending on the parameters. The *monostable* phenotype is characterized by the existence of a single, globally attracting, stable equilibrium. On the other hand, the *bistable* phenotype is characterized by the existence of two asymptotically stable equilibria and a single saddle equilibrium. As a reminder, the word “equilibrium” here refers generally to both the classical definition of an equilibrium for an ODE as well as the combinatorial equilibrium defined in Section 3.

5.1 The Toggle Switch Hill model

We begin by briefly outlining how the Hill model construction described in Section 2 yields a Hill function model associated with the ODEs in Equation (3). The Toggle Switch has two state variables of interest, denoted by x_1, x_2 , and thus the appropriate phase space is $X = (0, \infty)^2$. For $i = 1, 2$, the state variable x_i is assigned a positive linear decay parameter, γ_i . In addition, both edges of the network are assigned a negative Hill function since both edges in Figure 1(a) are repressing. These Hill functions contribute the additional 8 parameters to the model and the parameter space for the Toggle Switch Hill model is $\Lambda = (0, \infty)^{10}$. As described in Section 2, we collect the parameters into a vector which we order as follows

$$\lambda := (\gamma_1, \ell_{1,2}, \delta_{1,2}, \theta_{1,2}, d_{1,2}, \gamma_2, \ell_{2,1}, \delta_{2,1}, \theta_{2,1}, d_{2,1}) \in \Lambda.$$

Since each node of the Toggle Switch has only a single incoming edge we assign the interaction function defined by $p(z) = z$ to both coordinates of \mathcal{H} . Therefore, the Toggle Switch Hill model

is given by the formula

$$f(x, \lambda) = -\Gamma x + \mathcal{H}(x), \quad x \in X, \quad \lambda \in \Lambda \quad (13)$$

where the linear and nonlinear terms are given by

$$\Gamma = \begin{pmatrix} \gamma_1 & 0 \\ 0 & \gamma_2 \end{pmatrix} \quad \mathcal{H}(x) = \begin{pmatrix} H_{1,2}^-(x_2) \\ H_{2,1}^-(x_1) \end{pmatrix}. \quad (14)$$

As expected this is simply the vectorized form of the system of ODEs in Equation (3). Additionally, we note that f satisfies the hypotheses of Theorem 2 and consequently in the analysis to follow, Algorithm 2 was employed to bound the equilibria for the Toggle Switch. In fact, in Section 5.3 we prove a stronger version of Theorem 2 which improves the efficiency of our statistical investigation.

The relevant parameters for the combinatorial Toggle Switch model analyzed using DSGRN are as vectorized and denoted by

$$\xi := (\gamma_1, \ell_{1,2}, \delta_{1,2}, \theta_{1,2}, \gamma_2, \ell_{2,1}, \delta_{2,1}, \theta_{2,1}) \in \Xi,$$

where we remind the reader that $\Xi = (0, \infty)^8$ denotes the combinatorial parameter space which excludes the Hill coefficient parameters. Despite the fact that Ξ is 8 dimensional, DSGRN computes the combinatorial dynamics for the Toggle Switch in less than a second on a basic laptop. Recall from Section 1 that the combinatorial description of the dynamics consists of the 9 semi-algebraic sets listed in Table 1 and the Morse graph describing the combinatorial dynamics for all parameters in each of these 9 regions.

Finally, we relate the combinatorial and Hill model parameter spaces by defining the projection map $\pi_\Xi : \Lambda \rightarrow \Xi$ by the formula

$$\pi_\Xi(\gamma_1, \ell_{1,2}, \delta_{1,2}, \theta_{1,2}, d_{1,2}, \gamma_2, \ell_{2,1}, \delta_{2,1}, \theta_{2,1}, d_{2,1}) = (\gamma_1, \ell_{1,2}, \delta_{1,2}, \theta_{1,2}, \gamma_2, \ell_{2,1}, \delta_{2,1}, \theta_{2,1}).$$

In terms of this projection we can now restate the heuristic claims made at the end of Section 1. First, we claim that, with very high probability, $\lambda \in \Lambda$ is a bistable parameter for f if and only if $\pi_\Xi \lambda \in R(5)$. Then, let $\mathbf{r} : [0, 1] \rightarrow \Lambda$ be a path such that $d_{1,2} = d_{2,1} = 1$ at $\mathbf{r}(0)$, $d_{1,2}, d_{2,1} \gg 1$ at $\mathbf{r}(1)$, and $\pi_\Xi \circ \mathbf{r}$ is constant. Then we claim that with very high probability, we find a saddle-node bifurcation for f along \mathbf{r} if and only if $\pi_\Xi \circ \mathbf{r} \in R(5)$.

We will use statistical hypothesis testing combined with our efficient numerical implementation of the Toggle Switch to justify these two claims.

5.2 Reducing the number of parameters

While the full parameter space of the Toggle Switch can be studied by NDMA, we are interested in making the results more readable and easier to handle from a statistical perspective too. For this, we will make several changes to the model in order to reduce the dimension of the parameter space.

We will reduce the number of parameters via two mechanisms. First we will equate the Hill coefficients associated to both edges in the Toggle Switch. This amounts to assuming that $d := d_{1,2} = d_{2,1}$, is the common value of both Hill coefficients which reduces the number of parameters in the model by 1. Second, we will further reduce the dimension of the parameter space via non-dimensionalization of the parameters.

After identifying the Hill coefficients and performing non-dimensionalization whereby we may fix 3 parameter values to be $\gamma_1 = \theta_{2,1} = \theta_{1,2} = 1$ we obtain the *reduced Toggle Switch*

Hill model defined by

$$f^*(x) := \begin{pmatrix} -x_1 + \ell_{1,2}^* + \delta_{1,2}^* \frac{1}{1+x_2^d} \\ -\gamma_2^* x_2 + \ell_{2,1}^* + \delta_{2,1}^* \frac{1}{1+x_1^d} \end{pmatrix}. \quad (15)$$

where the parameters of the reduced model are related to the original parameters by the identities

$$\begin{aligned} \ell_{1,2}^* &:= \frac{\ell_{1,2}}{\gamma_1 \theta_{2,1}} \\ \delta_{1,2}^* &:= \frac{\delta_{1,2}}{\gamma_1 \theta_{2,1}} \\ \ell_{2,1}^* &:= \frac{\ell_{2,1}}{\gamma_1 \theta_{1,2}} \\ \delta_{2,1}^* &:= \frac{\delta_{2,1}}{\gamma_1 \theta_{1,2}} \\ \gamma_2^* &:= \frac{\gamma_2}{\gamma_1} \\ d &:= d_{1,2} = d_{2,1}. \end{aligned}$$

The parameter space associated to f^* is the subspace, $\Lambda^* \subset \Lambda$, defined by

$$\Lambda^* := \{\lambda \in \Lambda : \gamma_1 = \theta_{2,1} = \theta_{1,2} = 1, d_{1,2} = d_{2,1} = d\} \cong (0, \infty)^6,$$

and we denote a typical parameter by

$$\lambda^* := (\ell_{1,2}^*, \delta_{1,2}^*, \gamma_2^*, \ell_{2,1}^*, \delta_{2,1}^*, d) \in \Lambda^*.$$

The dynamics generated by f^* are conjugate to f restricted to the subset $\{\lambda \in \Lambda : d_{1,2} = d_{2,1}\}$ and therefore we have performed all computations described in the remaining sections using the reduced Toggle Switch model. We also note that the NDMAlibrary has been written to allow these sorts of constraints to be implemented just as easily as a general Hill model, and takes advantage of the reduced number of parameters for faster computation. However, it is crucial to point out that none of the algorithms in this paper rely on either of the reductions performed on this example.

After imposing these parameter constraints for the DSGRN parameter regions we obtain a *reduced* version of the combinatorial parameter space denoted by $\Xi^* := (0, \infty)^5 \subset \mathbb{R}^5$ where a typical reduced combinatorial parameter has the form $\xi^* = (\ell_{1,2}^*, \delta_{1,2}^*, \gamma_2^*, \ell_{2,1}^*, \delta_{2,1}^*)$. Observe that the 9 DSGRN parameter regions are projected onto semi-algebraic subsets of Ξ^* defined by the *reduced inequalities* given in the last column of Table 1. Of course, the dynamic phenotypes for each region are unchanged as a consequence of the conjugacy. Analogous to the discussion in Section 5.1 we define a projection map for the reduced parameter space $\pi_{\Xi^*} : \Lambda^* \rightarrow \Xi^*$ which is defined by projection onto the first 5 coordinates.

In the projected parameter space Ξ^* , we can readily define all the parameter regions already introduced by DSGRN in Λ^* in Section 5.1. The reduced inequalities for each projected region $R^*(i), i = 1, \dots, 9$ are presented in the last column of Table 1.

5.3 Numerical analysis of the Toggle Switch

Here we explicitly describe our implementation of numerical techniques described in Sections 4 for the Toggle Switch example starting with finding equilibria. For the case of the Toggle

Switch, some additional results are stated in Theorem 4. We begin by observing that f^* satisfies Definition 5 for any $\lambda^* \in \Lambda^*$ and therefore the bootstrap algorithm is applicable. Following the construction in Section 4.2 we obtain the bootstrap map for the reduced Toggle Switch which is given by the formula

$$\Phi(\alpha, \beta) = \begin{pmatrix} \ell_{1,2}^* + \frac{\delta_{1,2}^*}{1+\beta_2^d} \\ \frac{1}{\gamma_2^*} \left(\ell_{2,1}^* + \frac{\delta_{2,1}^*}{1+\beta_1^d} \right) \\ \ell_{1,2}^* + \frac{\delta_{1,2}^*}{1+\alpha_2^d} \\ \frac{1}{\gamma_2^*} \left(\ell_{2,1}^* + \frac{\delta_{2,1}^*}{1+\alpha_1^d} \right) \end{pmatrix} \quad (\alpha, \beta) \in \mathbb{R}^2 \times \mathbb{R}^2.$$

Following Algorithm 2 we start with the initial condition

$$(\alpha^{(0)}, \beta^{(0)}) := \begin{pmatrix} \ell_{1,2}^* \\ \ell_{2,1}^* \\ \ell_{1,2}^* + \delta_{1,2}^* \\ \ell_{2,1}^* + \delta_{2,1}^* \end{pmatrix},$$

and define the iterates under Φ by $(\alpha^{(n)}, \beta^{(n)}) = \Phi(\alpha^{(n-1)}, \beta^{(n-1)})$ for $n \geq 1$. Theorem 2 ensures that the sequence of iterates converges to a fixed point of Φ denoted by $(\hat{\alpha}, \hat{\beta}) \in \mathbb{R}^2 \times \mathbb{R}^2$ and that all equilibria of f^* are contained in the rectangle $[\hat{\alpha}_1, \hat{\beta}_1] \times [\hat{\alpha}_2, \hat{\beta}_2] \subset X$. However, in the case of the toggle switch we can prove a stronger version of Theorem 2 which we will exploit in our statistical analysis.

Theorem 4. *Let $f^* : X \rightarrow TX$ denote the Toggle Switch Hill model with $\lambda^* \in \Lambda^*$ fixed and let $\Phi : \mathbb{R}^4 \rightarrow \mathbb{R}^4$ be the associated bootstrap map for f^* . Suppose the orbit through $u^{(0)}$ converges to $\hat{u} := (\hat{\alpha}, \hat{\beta}) \in \mathbb{R}^2 \times \mathbb{R}^2$ and let $\hat{R} := [\hat{\alpha}_1, \hat{\beta}_1] \times [\hat{\alpha}_2, \hat{\beta}_2] \subset X$ denote the equilibrium bounds guaranteed by Theorem 2. Then exactly one of the following is true.*

1. *\hat{R} is a degenerate rectangle (i.e. for $i = 1, 2$, $\hat{\alpha}_i = \hat{\beta}_i$) and f^* has a unique equilibrium $\hat{x} = (\hat{\alpha}_1, \hat{\alpha}_2)$ which is stable.*
2. *\hat{R} is non-degenerate and f^* has at least two stable equilibria. Specifically, the corners of \hat{R} with coordinates*

$$\hat{x}_1 = (\hat{\alpha}_1, \hat{\beta}_2), \quad \hat{x}_2 = (\hat{\beta}_1, \hat{\alpha}_2)$$

are stable equilibria of f^ .*

Proof. Define $\hat{x}_1 := (\hat{\alpha}_1, \hat{\beta}_2)$, $\hat{x}_2 := (\hat{\beta}_1, \hat{\alpha}_2)$, and observe that since $(\hat{\alpha}, \hat{\beta})$ is a fixed point of Φ we have by direct computation

$$\begin{aligned} H_{1,2}(\hat{\beta}_2) &= \hat{\alpha}_1 \\ H_{2,1}(\hat{\beta}_1) &= \gamma_2^* \hat{\alpha}_2 \\ H_{1,2}(\hat{\alpha}_2) &= \hat{\beta}_1 \\ H_{2,1}(\hat{\alpha}_1) &= \gamma_2^* \hat{\beta}_2. \end{aligned}$$

It follows that

$$\begin{aligned} f^*(\hat{x}_1) &= f^*(\hat{\alpha}_1, \hat{\beta}_2) = \begin{pmatrix} \hat{\alpha}_1 - H_{1,2}(\hat{\beta}_2) \\ \gamma_2^* \hat{\beta}_2 - H_{2,1}(\hat{\alpha}_1) \end{pmatrix} = \begin{pmatrix} 0 \\ 0 \end{pmatrix} \\ f^*(\hat{x}_2) &= f^*(\hat{\beta}_1, \hat{\alpha}_2) = \begin{pmatrix} \hat{\beta}_1 - H_{1,2}(\hat{\alpha}_2) \\ \gamma_2^* \hat{\alpha}_2 - H_{2,1}(\hat{\beta}_1) \end{pmatrix} = \begin{pmatrix} 0 \\ 0 \end{pmatrix} \end{aligned}$$

so that \hat{x}_1, \hat{x}_2 are equilibria for f^* . Evidently, if \hat{R} is degenerate then $\hat{x}_1 = \hat{x}_2$ and by Theorem 2 it follows that this is the unique equilibrium for f^* . On the other hand if \hat{R} is nondegenerate then \hat{x}_1 and \hat{x}_2 are distinct equilibria of f^* .

Next, we prove that \hat{x}_1 is stable as the argument for stability of \hat{x}_2 is similar. Observe that the derivative of f^* at \hat{x}_1 is given by the formula

$$Df^*(\hat{x}_1) = \begin{pmatrix} -1 & H'_{1,2}(\hat{\beta}_2) \\ H'_{2,1}(\hat{\alpha}_1) & -\gamma_2^* \end{pmatrix}$$

which has eigenvalues satisfying

$$z^2 + (1 + \gamma_2^*)z + \gamma_2^* - H'_{1,2}(\hat{\beta}_2)H'_{2,1}(\hat{\alpha}_1) = 0. \quad (16)$$

Observe that since $H_{1,2}$ and $H_{2,1}$ are monotonically decreasing, the discriminant of the polynomial in Equation (16) is

$$(1 + \gamma_2^*)^2 - 4(\gamma_2^* - H'_{1,2}(\hat{\beta}_2)H'_{2,1}(\hat{\alpha}_1)) = (1 - \gamma_2^*)^2 + H'_{1,2}(\hat{\beta}_2)H'_{2,1}(\hat{\alpha}_1) > 0.$$

Hence, we can deduce that the eigenvalues are real and distinct and thus \hat{x}_1 is hyperbolic. Consequently, $Df^*(\hat{x}_1)$ has two linearly independent eigenvectors which we denote by $\mathbf{v}_1, \mathbf{v}_2$.

Let f_1, f_2 denote the two components of f^* . We consider points $x = (x_1, x_2)$ near the equilibrium at \hat{x}_1 lying on the lines defined by $x_1 = \hat{\alpha}_1$ and $x_2 = \hat{\beta}_2$. Specifically, we have the four cases:

1. If $x_1 < \hat{\alpha}_1$, then $f_1(x_1, \hat{\beta}_2) = -x_1 + H_{1,2}(\hat{\beta}_2) > -\hat{\alpha}_1 + H_{1,2}(\hat{\beta}_2) = 0$.
2. If $x_1 > \hat{\alpha}_1$, then $f_1(x_1, \hat{\beta}_2) = -x_1 + H_{1,2}(\hat{\beta}_2) < -\hat{\alpha}_1 + H_{1,2}(\hat{\beta}_2) = 0$.
3. If $x_2 < \hat{\beta}_2$, then $f_2(\hat{\alpha}_1, x_2) = -\gamma_2^*x_2 + H_{2,1}(\hat{\alpha}_1) > -\gamma_2^*\hat{\beta}_2 + H_{2,1}(\hat{\alpha}_1) = 0$.
4. If $x_2 > \hat{\beta}_2$, then $f_2(\hat{\alpha}_1, x_2) = -\gamma_2^*x_2 + H_{2,1}(\hat{\alpha}_1) < -\gamma_2^*\hat{\beta}_2 + H_{2,1}(\hat{\alpha}_1) = 0$.

Consequently, if $\epsilon > 0$ is sufficiently small, then f^* is transverse to the boundary of the ball

$$B_\epsilon(\hat{x}_1) := \{x \in \mathbb{R}^2 : \|x - \hat{x}_1\| < \epsilon\}$$

and the flow generated by f^* is in-flowing. It follows from continuity of f^* that there exists $\epsilon > 0$ sufficiently small such that the flow restricted to the subspaces $\text{span}\{\mathbf{v}_1\}$ and $\text{span}\{\mathbf{v}_2\}$ is also in-flowing. Hence, \mathbf{v}_1 and \mathbf{v}_2 lie in the stable manifold of \hat{x}_1 . \square

5.4 Statistical analysis of saddle nodes

Having built numerical methods to search for saddle nodes in the Toggle Switch, we now perform a statistical investigation of their results. Specifically, we investigate the accuracy of the dynamical phenotypes predicted using DSGRN as well as the effectiveness of our algorithm for numerically finding saddle-node bifurcations based on those predictions. We begin with the observation that if $d = 1$, then f^* has a unique equilibrium which is stable.

From our previous discussion of the Toggle Switch 5, given a parameter $\pi_{\Xi^*}\lambda^* = (\ell_{1,2}^*, \delta_{1,2}^*, \gamma_2^*, \ell_{2,1}^*, \delta_{2,1}^*)$ and a path $\mathbf{r} : [1, \infty] \rightarrow \Lambda^*$ defined by $\mathbf{r}(s) = (\ell_{1,2}^*, \delta_{1,2}^*, \gamma_2^*, \ell_{2,1}^*, \delta_{2,1}^*, s)$, if the DSGRN prediction were perfectly accurate then we would expect the following statements to hold:

1. If $\pi_{\Xi^*}\lambda^* \in R^*(5)$, then f^* undergoes a saddle-node bifurcation along the parameterized path \mathbf{r} .

2. If $\pi_{\Xi^*} \lambda^* \notin R^*(5)$, then f^* doesn't undergo a saddle-node bifurcation along \mathbf{r} .

Considering the non-linearity introduced by following the path \mathbf{r} , we have to consider these statements from a statistical perspective, that is: most paths \mathbf{r} that connect $R^*(5) \times \{\infty\}$ and $R^*(5) \times \{1\}$ undergo a numerical saddle node.

These two previous statements can be summarized by the following statistical statement: there is a correlation between the existence of a saddle node for λ^* and $\lambda^* \in R(5)$.

Using the numerical algorithms described in this paper and Theorem 4 we quantify the strength of this correlation using a χ^2 test with the null hypothesis being that no correlation exists. To describe the categorical random variables of the test we introduce some additional notation.

We start by randomly sampling parameters from Ξ^* and denote these samples by $\{\xi_1^*, \dots, \xi_N^*\}$. For each sample parameter, we check whether or not it lies in $R^*(5)$ and whether or not we detect a saddle-node bifurcation along \mathbf{r} . On this basis we form 4 mutually exclusive categories. We let

1. $p_s^{(5)}$ denotes the number of parameters in $R^*(5)$ undergoing a saddle-node bifurcation,
2. $p_m^{(5)}$ denotes the number of monostable parameters in $R^*(5)$ which do not undergo a saddle node bifurcation,
3. p_s^C denotes the number of parameters in the complement of $R^{(5)}$ undergoing a saddle-node bifurcation,
4. p_m^C denotes the number of monostable parameters in the complement of $R^{(5)}$ which do not undergo a saddle-node bifurcation.

Remark 4. An important element to discuss is the distribution of the chosen sample. For the Toggle Switch, a Gaussian distribution is created, such that each sample is the square of sample from said distribution. The variance and covariance matrix are chosen such that the probability of a sample being in either of the nine DSGRN regions $R(i), i = 1, \dots, 9$ is (roughly) equal. For bigger networks, such a distribution is hard to achieve, but in the Toggle Switch case we are able to find distributions such that the best sampled region has roughly the double of the number of samples as the worst sampled region. Let us remind that each region is unbounded, and no uniform sampling can be achieved. This justifies the use of unbounded distributions. The data-set for the Toggle Switch is created in the function `create_dataset.ToggleSwitch`.

The computation of the values in step 1-4 creates the following correlation matrix

$$M = \begin{pmatrix} p_s^{(5)} & p_s^C \\ p_m^{(5)} & p_m^C \end{pmatrix}.$$

Once the matrix M is assembled, we are able to use them to compute the χ^2 -test, []. This test is meant to prove that there is a correlation between a parameter being in R_5 and such parameter undergoing a saddle node. The smaller the p -value of the test, the stronger the correlation is expected to be.

In `toggle_switch_chi_test`, a sample from a random distribution is built, such that there are roughly equal number of sample points in $R(5)$ and its complement. Then, the matrix M is built. While each run the exact values might differ due to the sampling, a computation run on 10^4 produced

$$M = \begin{pmatrix} 1116 & 36 \\ 74 & 8685 \end{pmatrix},$$

together with Figures 5. While the code computes a data-set of this size in less than 5 minutes on a laptop, choosing larger data-sets would not give us better results, but the clarity of the figures would be impacted.

Thus, 93.7% of parameters in $R(5)$ undergo a saddle node with Hill coefficient under 100, compared to 0.4% outside of $R(5)$. Then, a χ -square test is run with M as input, giving a p -value of 0. This value is a statistical guarantee that combinatorial saddles correspond to smooth saddles and our approach is able to find the majority of saddle nodes.

We remark that the values of M do not include the parameters for which we could find a change in the number of equilibria but for which Newton did not return a solution for the saddle node problem (7). These parameters were few (89) in our run and are the product of numerical artifacts, as such they should be considered as outliers in our discussion.

Remark 5. Increasing the maximum Hill coefficient considered increases the likelihood of finding saddle nodes in $R^*(5)$, but also the likelihood of outliers due to numerical instabilities at high Hill coefficient values.

6 Applications to bifurcation analysis

6.1 Multiple saddle-node bifurcations, hysteresis, and isolas

We conduct here a numerical investigation into the qualitative nature of bistability for the Toggle Switch model. We once present the simplest explanation for the attractors computed with DSGRN in Table 1. Specifically, for generic $\xi^* \in \Xi^*$ with $\pi_{\Xi^*}(\xi^*) \in R^*(5)$, then for “large” d we expect f^* to have three equilibria: two stable and one saddle. For all other parameters we expect to find a single globally stable equilibrium for all Hill coefficients. In the previous section we demonstrated that with overwhelming probability this simple assumption is correct. The most parsimonious situation for a generic parameter to exhibit such global dynamics would be the following:

- If $\pi_{\Xi^*}(\xi^*) \in R^*(5)$ then along a Hill path through ξ^* f^* undergoes a single saddle-node bifurcation. At this point the saddle and one of the stable equilibria collide and disappear.
- If $\pi_{\Xi^*}(\xi^*) \notin R^*(5)$, then f^* has a single globally stable equilibrium for all $d \in [1, \infty)$. In particular, f^* does not undergo any saddle-node bifurcations.

While the first part of this assumption has been discussed in the previous Section, we here want to investigate the behaviour of parameters outside $R^*(5)$. The second part of the assumption seems reasonable based not only on our previous statistical result but also on the following intuition. For $d > 2$ both Hill functions are sigmoidal with d controlling the incline of the steepest part of the sigmoid. Therefore, for the Toggle Switch with identified Hill coefficients, it seems reasonable to guess that the nullclines of f^* move “toward each other” monotonically as $d \rightarrow \infty$. This intuition is shown in Figure 3 and suggests that f^* may undergo at most one saddle-node bifurcation with respect to d . However, the techniques described in this paper provide the means to efficiently test this conjecture. Despite the fact that the parameter space is “high” dimensional, the combinatorial analysis suggests that if a counterexample exists, one might look for it near the boundary of $R^*(5)$. With this search strategy in mind and using the efficient numerical methods described in this work, we easily find parameters

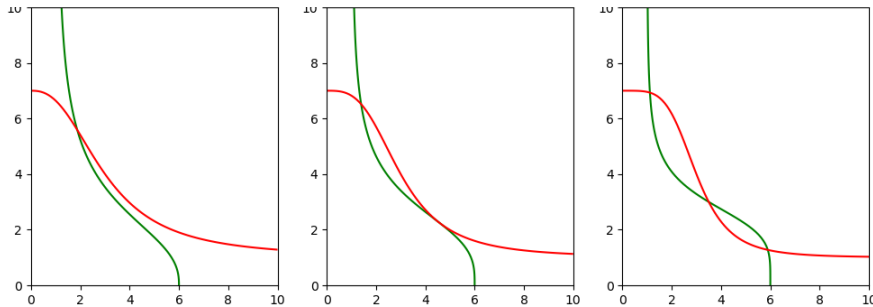


Figure 3: Toggle Switch nullclines for varying Hill coefficient along a Hill path. As the response of both Hill functions becomes steeper, the nullclines tend to be closer to one another until the saddle-node bifurcation at which point the nullclines intersect tangentially. Further increasing d increases the area bounded between the nullclines and the three equilibria appear to move further apart from each other.

which numerically demonstrate multiple bifurcations and surprisingly this conjecture appears to be false.

Indeed, the numerical investigation suggests that parameters outside of $R^*(5)$ may undergo (at least) two saddle-node bifurcations along a Hill path at some Hill coefficients $1 < d_1 < d_2 < \infty$. For Hill coefficients in $[1, d_1)$ and (d_2, ∞) , the system is monostable and bistable in (d_1, d_2) . This behavior is shown for two parameters in Figure 4. Moreover, the transition between monostability and bistability need not be hysteretic despite the fact that this model is a sort of “canonical” network motif associated with hysteretic switching. Indeed, pairs of saddle-node bifurcations occurring along a single Hill path may be hysteretic (i.e. connected by a single equilibrium branch) or form isolas which are disconnected from a “main” branch associated to stable equilibrium which persists for all Hill coefficients. The combination of these dynamic behaviors in this model suggests one possible cause for failures in the construction of synthetic biological switches. In Figure 4, we present a plot of the Hill coordinate with respect to the x_1 coordinate of numerically found equilibria for two different parameters outside of the center region. We can see how they differ in the fact that, in the first parameter, a continuous function can be plotted, while in the second one, the Hill coefficient is not a function of x_1 and creates an isolas. In both cases, the saddles have been first found numerically, then the equilibria have been numerically continued to produce the figures.

6.2 Degenerate saddle-node bifurcations

In this section we numerically investigate and compare the saddle-node bifurcations in the Toggle Switch occurring near the “corners” of $R(5)$. We note how the description of the attractors given by DSGRN also includes not only a count of the stable equilibria but their relative position in a simplified phase space. This richer information can be used to further investigate the dynamical behaviour supported by a system by applying our combined combinatorial-numerical approach.

In Section 6.2 we demonstrate how to deduce additional dynamical information in the Toggle Switch model. Consider the simplest situation that all of the attractors in the Morse decomposition identified for each region of the combinatorial parameter space in Table 1 is associated with a single stable equilibrium for some smooth vector field $f : (0, \infty)^2 \rightarrow \mathbb{R}^2$

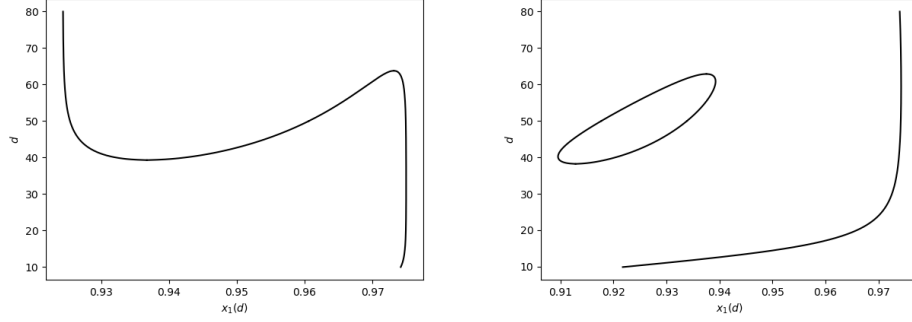


Figure 4: Branches of equilibria computed for the reduced Toggle Switch for varying d via pseudo-arc length continuation depicting the two mechanisms which cause multiple saddle-node bifurcations. (Left) Hysteretic behaviour for the Toggle Switch found at parameter value $\lambda^* = [0.9243, 0.0506, 0.8125, 0.0779, 0.8161]$. (Right) An isola is found at $\lambda^* = [0.6470, 0.3279, 0.9445, 0.5301, 0.3908]$ indicating that multiple saddle-node bifurcations are possible without hysteretic switching.

located in the indicated quadrant of the state space. We consider first a path through the continuous parameter space which visits the parameter regions in the order $R(5) \mapsto R(8) \mapsto R(7) \mapsto R(4) \mapsto R(5)$. In the combinatorial system, a continuous branch of equilibria can not cross the hyperplanes defined by the equations $x_1 = \gamma_1 \theta_{2,1}$ and $x_2 = \gamma_2 \theta_{1,2}$. Therefore, if f is a faithful continuous representation of the combinatorial dynamics then the most parsimonious explanation for the sequence of Morse decompositions along this path is as follows.

For parameters in $R(5)$, f has (at least) one unstable equilibrium. When passing between regions $R(5)$ and $R(8)$, this unstable equilibrium and the stable equilibrium in $(1, 0)$ disappear in a saddle-node bifurcation. Similarly, when passing between regions $R(5)$ and $R(4)$ this unstable equilibrium and the stable equilibrium in $(0, 1)$ disappear in a saddle-node bifurcation. Therefore, along the boundary separating $R(4)$ and $R(7)$ these two saddle-node bifurcations collide in a codimension-2 cusp bifurcation and similarly on the boundary between $R(8)$ and $R(7)$. An analogous analysis of a path visiting the regions (in order) $R(5) \mapsto R(2) \mapsto R(3) \mapsto R(6) \mapsto R(5)$ suggests another cusp bifurcation at the “corner” shared by $R(5)$ and $R(3)$.

To contrast this behavior, consider a path visiting the parameter regions $R(5) \mapsto R(8) \mapsto R(9) \mapsto R(6) \mapsto R(5)$. For all regions along this path, the unique stable equilibrium is located in quadrant $(0, 1)$ which is most likely modelled by the existence of a common smooth branch of equilibria which remains in this quadrant throughout the path. On the boundary between $R(5)$ and $R(6)$, the unstable equilibrium and the stable equilibrium in $(1, 0)$ disappear in a saddle-node bifurcation much like on the boundary between $R(5)$ and $R(8)$. A similar situation occurs for paths visiting regions $R(5) \mapsto R(2) \mapsto R(1) \mapsto R(4) \mapsto R(5)$. This behaviour is not likely compatible with a cusp bifurcation at the “corner” between $R(5)$ and $R(1)$ or $R(9)$. Thus, our conjecture is that bifurcations for parameters at the “corners” shared by region $R(5)$ and regions $R(1), R(9)$ and those at the corners shared by $R(5)$ and regions $R(3), R(7)$ are caused by very different mechanisms.

To investigate our conjecture, suppose once again that f^* is the nondimensionalized Toggle Switch Hill model defined in section 5.2 with 6 dimensionless parameters. For visualisation purposes, we define a suitable dimension reduction map from from Λ^* onto the rectangle

$[0, 3]^2 \subset \mathbb{R}^2$ which preserves these 9 DSGRN parameter regions and the relative distances between parameters and the region boundaries.

To start, suppose $\xi^* \in \Xi^*$ and define the related parameters $\{a_1, b_1, a_2, b_2\}$ by the formulas

$$a_1 := \ell_{1,2}^* \quad b_1 := \ell_{1,2}^* + \delta_{1,2}^* \quad a_2 := \frac{\ell_{2,1}^*}{\gamma_2^*} \quad b_2 := \frac{\ell_{2,1}^* + \delta_{2,1}^*}{\gamma_2^*}.$$

Observe that if the reduced polynomial inequalities in Table 1 are expressed in terms of these new parameters, then the 9 DSGRN parameter regions as well as their boundaries are defined by linear manifolds. For example, region $R(5)$ is given by

$$R(5) = \{(a, b) \in \mathbb{R}^2 \times \mathbb{R}^2 : 0 < a_1 < 1 < b_1 \text{ and } 0 < a_2 < 1 < b_2\}$$

and the boundary separating $R(5)$ and $R(6)$ is given by

$$\partial R(5) \cap \partial R(6) = \{(a, b) \in \mathbb{R}^2 \times \mathbb{R}^2 : 0 < a_1 < 1 < b_1, a_2 = 1, \text{ and } 1 < b_2\}.$$

Implicitly this defines a nonlinear transformation $\psi : \Xi^* \rightarrow \mathbb{R}^2 \times \mathbb{R}^2$ given by the formula $\psi(\xi^*) = (a, b)$ which maps each DSGRN region to a unique hyperplane in $\mathbb{R}^2 \times \mathbb{R}^2$.

To complete the construction, fix positive constants \bar{a}, \bar{b} and define another map $g : \mathbb{R}^2 \times \mathbb{R}^2$ by the formulas

$$g_1(a, b) = \begin{cases} b_2 & \text{if } b_2 \leq 1 \\ 1 + \frac{1-a_2}{b_2-a_2} & \text{if } a_2 < 1 < b_2 \\ 2 + \frac{a_2-1}{\bar{a}-1} & \text{if } 1 \leq a_2 \end{cases} \quad g_2(a, b) = \begin{cases} b_1 & \text{if } b_1 \leq 1 \\ 1 + \frac{1-a_1}{b_1-a_1} & \text{if } a_1 < 1 < b_1 \\ 2 + \frac{a_1-1}{\bar{a}-1} & \text{if } 1 \leq a_1 \end{cases} \quad (17)$$

Observe that the bounded subset $K_{\bar{a}, \bar{b}} \subset \text{image } \psi$ defined by the formula

$$K_{\bar{a}, \bar{b}} := \{(a, b) \in \text{image } \psi : \|a\|_\infty \leq \bar{a}, \|b\|_\infty \leq \bar{b}\}.$$

we have that $g(K_{\bar{a}, \bar{b}}) \subset [0, 3]^3$.

We use the previous constructions to visualize the relative position of parameters as follows. Given a fixed collection of parameters $\{\xi_1^*, \dots, \xi_M^*\} \subset \Xi^*$ we choose \bar{a}, \bar{b} sufficiently large so that $\psi(\xi_j^*) \in K_{\bar{a}, \bar{b}}$ for $1 \leq j \leq M$. Therefore, the mapping $g \circ \psi : \Xi^* \rightarrow [0, 3]^2$ satisfies the following properties.

1. Each of the 9 parameter regions is mapped to a distinct unit square in $[0, 3]^2$ and their relative positions are preserved. In fact, $g \circ \psi$ has been constructed so that the images of these regions are simply obtained by superimposing the graph in Figure 1(b) onto $[0, 3]^2$. We let $S(i) := g \circ \psi(R^*(i))$ denote these unit squares for $1 \leq i \leq 9$.
2. Each boundary separating a pair of parameter regions is mapped into a line of the form $g_i = j$ with $i \in \{1, 2\}$ and $j \in \{1, 2, 3\}$. In other words, boundaries of parameter regions are mapped onto boundaries of the corresponding unit square and relative positions of the boundaries are also preserved.
3. Relative proximity to boundaries is preserved. Specifically, suppose $\xi_1, \xi_2 \in R^*(j)$ and $\text{dist}(\xi_1, \partial R(j)) < \text{dist}(\xi_2, \partial R(j))$, then $\text{dist}(g \circ \psi(\xi_1), \partial S(j)) < \text{dist}(g \circ \psi(\xi_2), \partial S(j))$.

Given this projection of the parameter space into a two-dimensional Euclidean space we now visually investigate the behavior of saddle-node bifurcations along the boundary of $R^*(5)$.

To generate random parameters for a statistical analysis, we construct an unbounded distribution \mathcal{F} such that samples taken from \mathcal{F} span the parameter regions $R(i) \subset \Xi^*, i =$

1, ..., 9 of the Toggle Switch in such a way that no region is significantly over- or under-represented. Thus, we create large samples of parameters knowing that $R(5)$ will be roughly represented in the sample as often as the other parameter regions. Having constructed a large sample of parameters, we can use the techniques presented in this Section to project each parameter to the square $[0, 3]^2$. For each parameter sample $\lambda \in \Xi^*$, we are interested in finding any saddle node bifurcation that happens along the path $\mathbf{r}(s)$ as presented in Section 5.3. We will restrict ourselves to Hill coefficients satisfying $1 \leq d \leq 100$, since higher Hill coefficients would give rise to numerical instability.

The first visual result we want to present is an overview of parameters that undergo saddle nodes at different Hill coefficients. For this, we find saddle nodes with respect to the Hill coefficient, then project the parameter over the $[0, 3]^2$ square and represent the Hill coefficient as a heat map. In Figure 5, on the left the projection 17 is used, while the color indicates the lowest Hill coefficient d for which we could find a saddle node at the given parameter value. On the right Figure, there is a scatter plot of all parameters considered. These includes information on parameters that never undergo a saddle node, but also on parameters that undergo more than one saddle node. We will investigate further this class of parameters in Section 6.

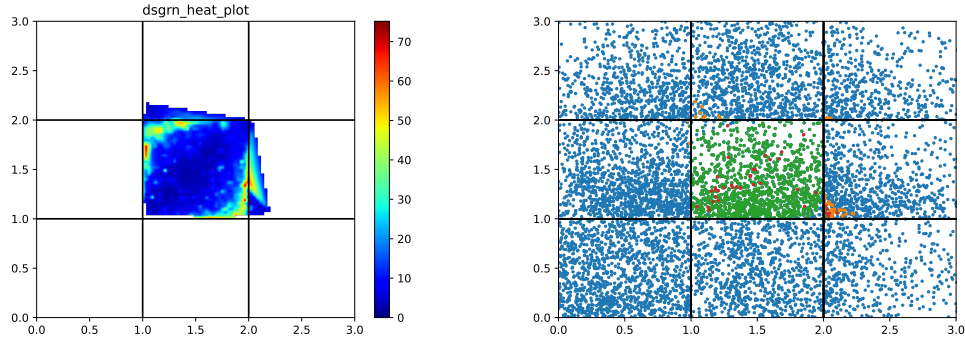


Figure 5: Left: Using the projection presented in Equation 17, a heat map is plotted, indicating the smallest Hill coefficient undergoing a saddle node. Right: Using the same projection, parameters are plotted in blue if they don't undergo any saddle node, in green if they undergo a single saddle node, in orange if they undergo multiple saddle nodes and in red if the bisection algorithm found a saddle node that was not numerically confirmed with Equation (7)

At first glance, Figure 5 gives an intuition of what we proved in Section 5.4: choosing parameters in $R^*(5)$ has the highest likelihood of giving us a saddle node for relatively low Hill coefficient. Looking at this map, we observe that the bottom left of the center region seems to be the best location for a practical bistable switch, since most parameters in that section undergo a saddle node at low Hill coefficient, and thus support bistability for most large Hill coefficients. We notice how there are saddle nodes taking place outside the center region, but most of them undergo two saddle nodes, thus for high enough Hill coefficient they again present a unique stable fixed point, as discussed in Section 6.1.

Crucially, this plot supports the claim that saddle-node bifurcations disappear into a cusp (or other codimension-2) bifurcation along a loop around the points $(1, 1)$ or $(2, 2)$. However, along a loop around $(1, 2)$ or $(2, 1)$, saddle-node bifurcations seem to disappear “at infinity”. This is consistent with the observations we obtained from only the combinatorial dynamics

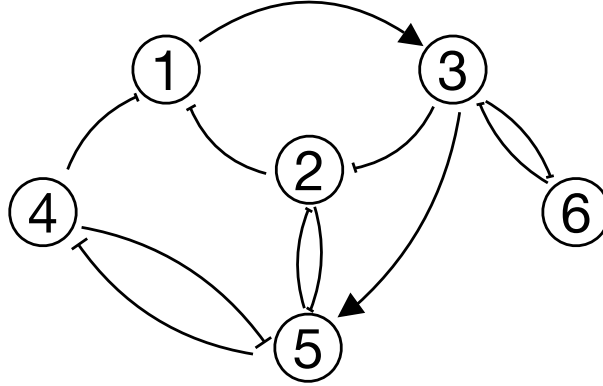


Figure 6: The network structure for the EMT model associated with the Hill model given in Equation (18)

using DSGRN, and that we presented at the beginning of this Section.

6.3 A high dimensional example: the EMT model

As a final example we demonstrate the ability to reliably identify bistability and find saddle-node bifurcations even in “very high” dimensional parameter models. In [20] the authors study a model for the Epithelial-Mesenchymal Transition network shown in figure 6. We identify the 6 genes in this network with state variables defined by

$$\begin{array}{lll} x_1 : \text{TGF}\beta & x_2 : \text{miR200} & x_3 : \text{Snail1} \\ x_4 : \text{Ovol2} & x_5 : \text{Zeb1} & x_6 : \text{miR35a} \end{array}$$

The associated Hill model for this network denoted by f is defined on the state space $X := [0, \infty)^6$. As expected the linear part of this model has parameters $\gamma_1, \dots, \gamma_6$ representing the linear decay rate of each of the 6 state variables. Under the assumption that all activating edges correspond to addition in the interaction function and all repressing edges are multiplied, the nonlinear term denoted by $\mathcal{H}(x)$ is defined by

$$\mathcal{H}(x) := \begin{pmatrix} H_{1,2}^-(x_2)H_{1,4}^-(x_4) \\ H_{2,3}^-(x_3)H_{2,5}^-(x_5) \\ H_{3,1}^+(x_1)H_{3,6}^-(x_6) \\ H_{4,5}^-(x_5) \\ H_{5,2}^-(x_2)H_{5,3}^+(x_3)H_{5,4}^-(x_4) \\ H_{6,3}^-(x_3)H_{6,5}^-(x_5) \end{pmatrix} \quad (18)$$

$H_{i,j}^*$ denotes a Hill function associated to the edge from node i to node j which contributes 4 non-negative parameters. Therefore the associated parameter space for this Hill model is $\Lambda = (0, \infty)^{54}$.

In order to analyze this model using the tools discussed in this work we first implement this model in DSGRN. The combinatorial parameter space has 10,368,000,000 regions and we begin by finding a parameter region P_M , which exhibits combinatorial monostability and has a neighboring region P_B exhibiting combinatorial bistability. Considering how widespread such regions seems to be, we don't check all possible regions, but stop within the first 100.

Since P_M and P_B are semi-algebraic subset of \mathbb{R}^{42} described by hundreds of polynomial inequalities, we do not provide a list of these inequalities. However, these parameter regions have indices 302 and 284 in DSGRN and the interested reader can inspect these inequalities using the code available at <https://github.com/skepley/NDMA/releases/tag/version0>.

Due to the dimension of the parameter space and number of the parameter regions in this example it is not feasible to attempt any sort of statistical analysis of our accuracy. In fact, the purpose of this example is to demonstrate that we can even find saddle-node bifurcations in this model at all! With this in mind, we consider the reduced Hill model in which we identify the Hill coefficients for all 12 edges of the network. This is an ODE with 43 parameters, one of which is the common Hill coefficient which we denote by d .

From the two regions we selected, we are interested in creating a large enough sample of parameters. One of DSGRN functionalities allows us to assign the appropriate region to a parameter vector, another allows us to find one (non-random) parameter within any given region. To sample regions P_M and P_B , we first query DSGRN to provide us with one point in each region, p_m and p_b . We then create a multivariate Gaussian distribution around the segment connecting these two parameters. By sampling from this Gaussian distribution we create a point cloud mostly distributed in P_M , P_B and overlapping on neighbouring regions. We could choose a smaller variance to ensure all our samples belongs to the selected regions, but that would guarantee we are not spanning much of P_M and P_B either.

Thus, we randomly sampled 10,000 parameters from this Gaussian distribution. DSGRN computed that 7772 lie in P_M and 1231 lie in P_B , the remaining parameters were from outside both regions.

We can then numerically search for saddle nodes along the curve of increasing Hill coefficients for a subsample of these parameters. Due to the computational requests of this computation, a smaller subsample was considered, where the same number of random parameters were selected from the monostable and the bistable region. In this case, we can build a contingency matrix as discussed in Section 5.4, where we replace $R(5)$ with the bistable region and its complement with the monostable region. No sample outside of these two regions is considered. Due to the increased size of the problem, a longer computational time is necessary, but we computed the following contingency matrix for a subsample of 200 parameters:

$$M = \begin{pmatrix} 5 & 0 \\ 194 & 100 \end{pmatrix},$$

where a single parameter could not be determined. Here we can see that roughly 2.5% of the parameters in the bistable region undergo a saddle node, while none of the parameters in the monostable region do. The χ -test for this contingency matrix returns a p -value of 0.07. While it doesn't breach the traditional threshold of 0.05, we are confident this should be a good indication to support our method. The code is presented in `EMT_chitest.py`.

The parameters and computations for both the parameters in P_m and P_B are available at <https://github.com/skepley/NDMA/releases/tag/version0>.

7 Conclusion

The goal of this paper is not only to resolve some dynamical questions on the behaviour of the Toggle Switch, but most notably to present an initial step towards the integration of combinatorial and numerical methods in the study of global dynamics. Indeed, using purely combinatorial information provided by DSGRN we can deduce significant information about the dynamics for any smooth version of the Toggle Switch. These claims are compounded by the development of NDMA, a library centered around a fast parameter search in smooth switching systems. A method for reliably finding all equilibria in systems with sigmoidal non-linearities is presented, that allows for a reliable and vast saddle node search. While for the implementation Hill models are used (Section 2), we underline how this was a purely computational choice, and all the theoretical background and methodology proposed here are independent of the chosen non-linearity.

Two main examples of the proposed methodology are presented. At first, an in-depth study of the Toggle Switch is carried out. This study not only supports the statement that the analysis of switching systems provides incredibly useful information for a parameter search, but highlights some numerically discovered dynamical behaviour in the Toggle Switch: notably the existence of a codimension-2 cusp bifurcations and the existence of isolas, together with the disappearance of saddle nodes at infinity.

Having developed this toy problem, we then get our hands on a more complex system: the EMT model. Here, the high dimensional parameter space, counting 54 parameters, is so vast that most statistical approaches would not be able to sample it satisfactorily. Using the information provided by DSGRN on the presence of monostable and bistable regions in the switching system, we are able to find bistability in the smooth system, proven by the existence of saddle nodes.

Furthermore, we have strong statistical support for the presence of saddle nodes in the regions selected with DSGRN is statistically significantly different from their presence in other regions. This is of great impact in applications: it is now possible to search for parameters supporting a chosen dynamical signature by using combinatorial information on switching systems.

References

- [1] Carmen Chicone. *Ordinary differential equations with applications*, volume 34 of *Texts in Applied Mathematics*. Springer, New York, second edition, 2006.
- [2] Bree Cummins, Tomas Gedeon, Shaun Harker, Konstantin Mischaikow, and Kafung Mok. Combinatorial Representation of Parameter Space for Switching Networks. *SIAM J. Appl. Dyn. Syst.*, 15(4):2176–2212, 2016.
- [3] William Duncan, Tomas Gedeon, Hiroshi Kokubu, Konstantin Mischaikow, and Hiroe Oka. Equilibria and their stability in networks with steep sigmoidal nonlinearities. *SIAM J. Appl. Dyn. Syst.*, 20(4):2108–2141, 2021.
- [4] Marcio Gameiro, Jean-Philippe Lessard, and Alessandro Pugliese. Computation of smooth manifolds via rigorous multi-parameter continuation in infinite dimensions. *Found. Comput. Math.*, 16(2):531–575, 2016.
- [5] Timothy Gardner, Charles Cantor, and James Collins. Construction of a genetic toggle switch in escherichia coli. *Nature*, 403(6767):339–342, 2000.

- [6] Tomáš Gedeon, Bree Cummins, Shaun Harker, and Konstantin Mischaikow. Identifying robust hysteresis in networks. *PLOS Computational Biology*, 14(4):1–23, 2018.
- [7] Tomáš Gedeon, Shaun Harker, Hiroshi Kokubu, Konstantin Mischaikow, and Hiroe Oka. Global dynamics for steep nonlinearities in two dimensions. *Phys. D*, 339:18–38, 2017.
- [8] Michael E. Henderson. Multiple parameter continuation: computing implicitly defined k -manifolds. *Internat. J. Bifur. Chaos Appl. Sci. Engrg.*, 12(3):451–476, 2002.
- [9] Allan Hungria, Jean-Philippe Lessard, and J Mireles James. Rigorous numerics for analytic solutions of differential equations: the radii polynomial approach. *Mathematics of Computation*, 85(299):1427–1459, 2016.
- [10] W. D. Kalies, K. Mischaikow, and R. C. A. M. VanderVorst. An algorithmic approach to chain recurrence. *Found. Comput. Math.*, 5(4):409–449, 2005.
- [11] W. D Kalies, K Mischaikow, and R.C.A.M. Vandervorst. Lattice structures for attractors II. *Found. Comput. Math.*, 1(2):1–41, 2015.
- [12] W. D Kalies, K Mischaikow, and R.C.A.M. Vandervorst. Lattice structures for attractors III. *J Dyn Diff Equat*, 2021.
- [13] William Kalies, Konstantin Mischaikow, and Robert Vandervorst. Lattice structures for attractors I. *J. of Comp. Dyn.*, 1(2), 2014.
- [14] Shane Kepley, Konstantin Mischaikow, and Lun Zhang. Computing linear extensions for polynomial posets subject to algebraic constraints. *SIAM J. Appl. Algebra Geom.*, 5(2):388–416, 2021.
- [15] Jean-Philippe Lessard. Rigorous verification of saddle-node bifurcations in odes. *Indagationes Mathematicae*, 27(4):1013–1026, 2016.
- [16] Jean-Philippe Lessard, JD Mireles James, and Julian Ransford. Automatic differentiation for fourier series and the radii polynomial approach. *Physica D: Nonlinear Phenomena*, 334:174–186, 2016.
- [17] Laurence M Levasseur, Harry K Slocum, Youcef M Rustum, and William R Greco. Modeling of the time-dependency of in vitro drug cytotoxicity and resistance. *Cancer Research*, 58(24):5749–5761, 1998.
- [18] Bree Cummins Marcio Gameiro, Shaun Harker. Dsgrn: Dynamic signatures generated by regulatory networks. <https://github.com/marciogameiro/DSGRN>, 2020.
- [19] Jan van den Berg, Jean-Philippe Lessard, and Konstantin Mischaikow. Global smooth solution curves using rigorous branch following. *Mathematics of Computation*, 79(271):1565–1584, 2010.
- [20] Ying Xin, Bree Cummins, and Tomáš Gedeon. Multistability in the epithelial-mesenchymal transition network. *BMC Bioinformatics*, 21, 2020.
- [21] Bo Yan, Joseph M Chalovich, Bernhard Brenner, et al. Theoretical kinetic studies of models for binding myosin subfragment-1 to regulated actin: Hill model versus geeves model. *Biophysical Journal*, 80(5):2338–2349, 2001.